

How Far Have We Gone in Generative Image Restoration? A Study on its Capability, Limitations and Evaluation Practices

Xiang Yin¹, Jinfan Hu^{2,4}, Zhiyuan You^{2,3}, Kainan Yan^{2,4}, Yu Tang², Chao Dong^{2,5,6}, Jinjin Gu⁷

¹Fudan University ²Shenzhen Institutes of Advanced Technology, Chinese Academy of Sciences

³Multimedia Laboratory, The Chinese University of Hong Kong ⁴University of the Chinese Academy of Sciences

⁵Shanghai AI Laboratory ⁶Shenzhen University of Advanced Technology ⁷INSAIT, Sofia University “St. Kliment Ohridski”

<https://github.com/yxyuanxiao/how-far-have-we-gone>

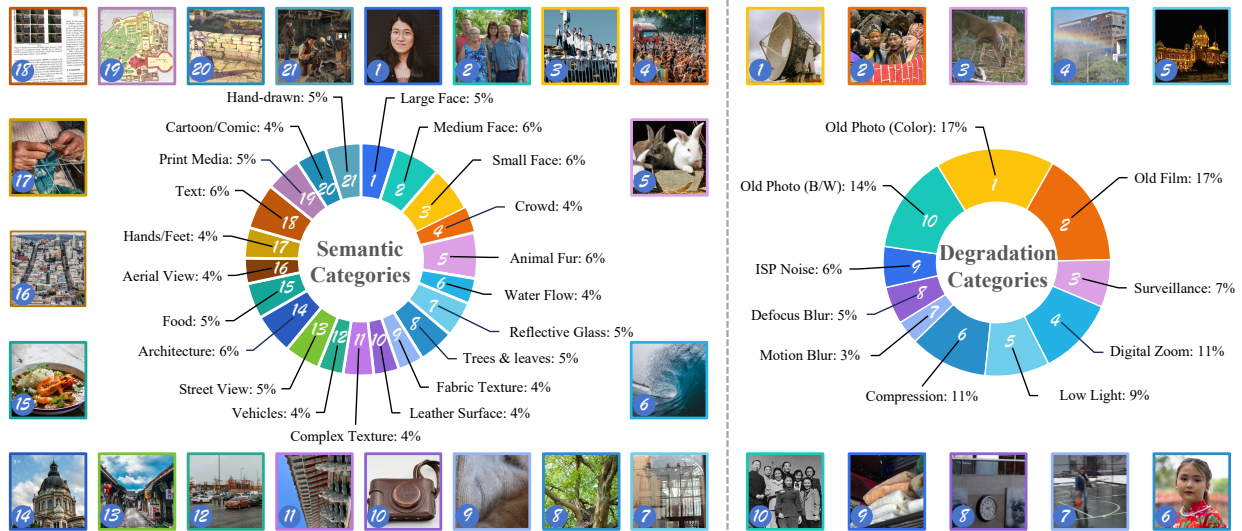


Figure 1. Overview of the proposed dataset composition across **Semantic** and **Degradation** dimensions. The semantic categories (left) cover diverse visual contents to reveal the perceptual and structural challenges faced by generative restoration models. The degradation categories (right) reflect real-world conditions where restoration models are typically applied.

Abstract

Generative Image Restoration (GIR) has achieved impressive perceptual realism, but how far have its practical capabilities truly advanced compared with previous methods? To answer this, we present a large-scale study grounded in a new multi-dimensional evaluation pipeline that assesses models on detail, sharpness, semantic correctness, and overall quality. Our analysis covers diverse architectures, including diffusion-based, GAN-based, PSNR-oriented, and general-purpose generation models, revealing critical performance disparities. Furthermore, our analysis uncovers a key evolution in failure modes that signifies a paradigm shift for the perception-oriented low-level vision field. The central challenge is evolving from the previous problem of detail scarcity (under-generation) to the new frontier of detail quality and semantic control (preventing over-generation). We also leverage our benchmark to train a new IQA model

that better aligns with human perceptual judgments. Ultimately, this work provides a systematic study of modern generative image restoration models, offering crucial insights that redefine our understanding of their true state and chart a course for future development. The code is available

1. Introduction

Generative image restoration (GIR) has brought remarkable progress to the field of image restoration. By leveraging generative priors, recent models [1–6] achieve visually realistic and perceptually pleasing restoration results, producing fine textures and details unattainable by conventional methods [7]. At the same time, these methods seem to exhibit strong generalization, performing surprisingly well even on unseen or mixed degradations. However, this powerful generative capacity, while beneficial, also raises fundamental questions about the fidelity and controllability of restored content, especially when applied to real-world

degradations and diverse semantic categories. These issues, though increasingly prevalent, have not been systematically studied or adequately reflected. Focusing on GIR methods, particularly diffusion-based approaches, we aim to provide a comprehensive understanding of both the remarkable advances and the emerging risks of GIR.

Generative priors, the foundation of recent progress, can also be a double-edged sword. In earlier paradigms, restoration models lacked the ability to generate new content. By contrast, modern GIR models with strong generative capabilities can enhance realism but also lead to hallucinated details, structural distortions, and semantic inconsistencies. Controlling this generative capability has thus become a critical and challenging problem: the stronger the generative prior, the harder it is to balance realism and fidelity. Although modern GIR models perform the aforementioned tasks, yet a comprehensive understanding of when and why GIR models fail under different conditions is still missing.

Limitations lie in how current GIR models are evaluated. Existing benchmarks [8, 9] and IQA methods largely overlook semantic dependency, treating all scenes as equally difficult. Moreover, most existing datasets [10, 11] focus only on conventional synthetic degradations, such as downsampling, noise, compression, or blur. These degradations do not reflect the real-world conditions in which GIR models are commonly applied, such as Internet images, old films, and old photos. Furthermore, most assessments collapse image quality into a single numerical score, making it difficult to identify the underlying causes of failure.

In this paper, we present a systematic and fine-grained study of state-of-the-art image restoration models. Specifically, (1) we perform detailed analyses across both semantic scenes and degradation types, constructing a carefully balanced dataset with fine-grained semantic and degradation annotations; (2) we quantify image quality at a fine-grained level and go beyond simple scoring by categorizing the diverse failure patterns observed in GIR models; and (3) we use this dataset to train an image quality assessment (IQA) model capable not only of predicting perceptual quality but also of diagnosing the specific failure modes present in a restored image. Our study thus enables a more comprehensive and diagnostic understanding of GIR model performance and provides a foundation for future evaluation and the development of agent-based image restoration systems.

2. Related Work

Image Restoration (IR) aims to recover high-quality images from their degraded counterparts. Early methods focused on specific degradations such as denoising [12–14], deblurring [15–17], deraining [18, 19], and super-resolution [2, 20–24]. These models typically relied on hand-crafted priors or task-specific convolutional architectures [7], thus exhibiting limited generalization to unseen

degradations. With the rise of generative modeling, GAN-based IR methods [25–27] introduced adversarial objectives to enhance perceptual realism beyond pixel-level fidelity. Although GANs improved visual quality, they often generated unnatural textures and suffered from unstable training [7]. To overcome these limitations, diffusion-based generative models have recently emerged as a more stable and expressive alternative, demonstrating superior performance in both fidelity and diversity [7]. Recently, diffusion models [28, 29] have demonstrated remarkable generative capability and surpassed GANs in both fidelity and diversity. Recent studies [5, 6, 30–34] have further leveraged large-scale diffusion backbones for real-world image restoration, achieving photorealistic and semantically consistent results across diverse degradations.

Image Quality Assessment (IQA) plays a vital role in evaluating the perceptual quality of restored or generated images. IQA methods can be categorized into *full-reference* and *non-reference* types. Full-reference IQA approaches compute a similarity-based quality score between a distorted image and its corresponding high-quality reference. Classical methods like PSNR and SSIM [35] rely on hand-crafted perceptual metrics [36, 37]. Pioneered by LPIPS [38] and PieAPP [10], and supported by large-scale IQA datasets [11, 38–40], deep-learning methods [41–47] have achieved high accuracy in regressing perceptual quality scores. Non-reference IQA methods directly predict a quality score without requiring any reference. Early works relied on hand-crafted natural image statistics [48–54], while later deep-learning-based methods [55–67] replaced these handcrafted features with learned perceptual priors from human-annotated datasets [39, 68–70]. Recent methods incorporate vision-language models [71–77], enabling multimodal reasoning and richer perceptual understanding through textual semantics.

IQA for model-restored images. Most existing IQA models still struggle to capture subtle perceptual or semantic discrepancies introduced by modern generative restoration methods, as indicated by benchmarks like FGResQ [78], SRIQA-Bench [9], and ISRGen-QA [8]. Nonetheless, the coverage of these benchmarks remains limited, lacking coverage of the semantic and content-level variations introduced by modern generative restoration or generation models. In this work, we focus on the emerging challenge of evaluating *generative image restoration*, where both traditional and multimodal IQA methods fail to effectively capture hallucination tendencies and semantic shifts.

3. Evaluation Design

3.1. Dataset Collection

The datasets employed in previous benchmarks are typically constructed by mixing a wide variety of images from many categories, while treating the semantic content of each

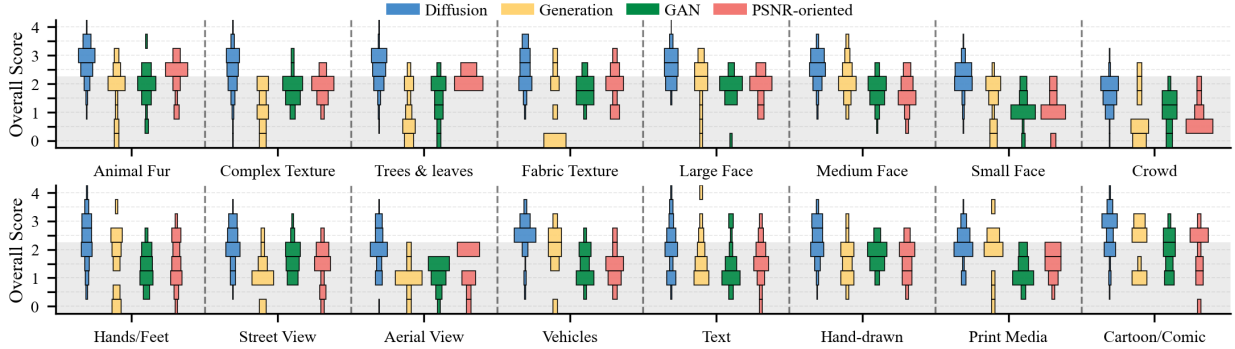


Figure 2. Distribution of annotated total scores across semantic scene groups. The horizontal width of each box indicates the percentage of samples within each score interval. The light gray region indicates low overall scores, representing generally unacceptable results.

image as incidental rather than a controlled factor. As a result, these benchmarks largely support only holistic analyses based on average performance metrics [8, 9], and offer little insight into how GIR models behave on different kinds of images. Such aggregate analysis is no longer sufficient for contemporary GIR models. Their integration of semantic understanding and generative capability leads to strongly semantic sensitive behavior, where performance can vary dramatically across categories such as text, hands, and faces [79–81]. Yet there is still no dedicated dataset or benchmark that systematically examines how semantic content and degradation type jointly affect model behavior. To fill this gap, we construct a new testset that deliberately balances diverse semantic categories and degradation types, with a particular focus on those that are known to be challenging for current GIR models.

Semantic categories. The semantic dimension of our dataset is curated with two principles: (1) the selected scenes should be challenging for current GIR models; and (2) they should cover content that is both perceptually salient to humans and diagnostically valuable for evaluating generative restoration quality. As illustrated in Fig. 1, our semantic categories span a wide range of human-centric, structural, texture-related, and symbolic scenes that comprehensively reflect real-world visual diversity. Human-centric categories such as *faces* and *hands/feet* are included. Their distinctive geometric structure and familiarity to humans, where even slight distortions or inconsistencies are easily noticeable and thus serve as clear indicators of restoration fidelity. Smaller faces suffer from severe degradation and rely more heavily on generative priors to reconstruct plausible features. While in the *crowd* category, numerous small, variably oriented faces further challenge a model’s ability to infer orientation and maintain facial geometry. Structure-related categories such as *vehicles*, *architecture*, *street view*, *aerial view* and *food* are included to evaluate a model’s capacity for geometric layout and spatial consistency. These categories cover both rigid and non-rigid structures, ranging from buildings and cars to food,

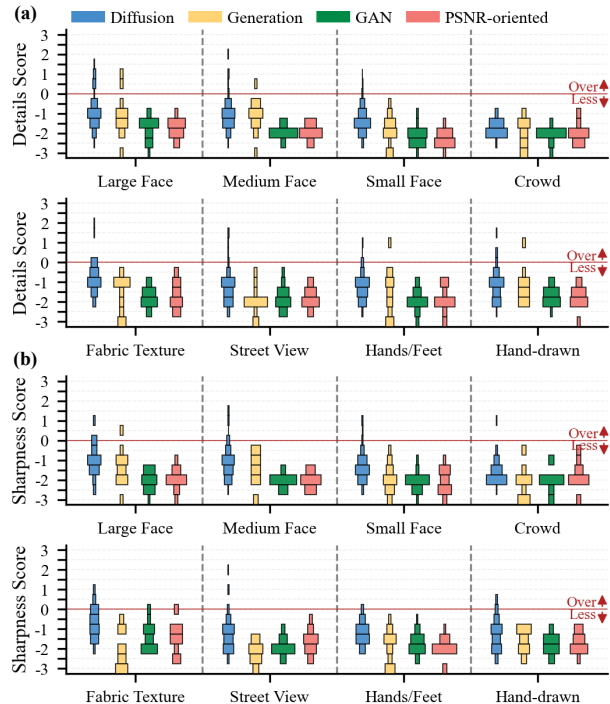


Figure 3. Detail and sharpness score distributions across semantic scenes. The width of each box corresponds to the percentage of samples. The red line indicates the balance point; scores above it (**Over** ↑) denote over-generation, and scores below it (**Less** ↓) denote under-generation.

and reflect how well models preserve perspective relations, proportions, and scene layouts under degradation. Texture-rich materials such as *animal fur*, *water flow*, *fabric*, *leather* and *trees & leaves* are included to assess whether models can generate fine-grained and coherent textures that appear both natural and physically plausible. We also include stylized and symbolic content such as *text*, *printed media*, *cartoons/comics*, and *hand-drawn*. These scenes emphasize the challenge of preserving semantic and stylistic fidelity, where text demands pixel-level precision for legibility, and artistic depictions require consistent style maintenance.

Degradation types. The treatment of degradation in previ-

Model	Architecture	Model	Architecture
HYPIR [6]	Diffusion-based	S3Diff [85]	Diffusion-based
SUPIR [5]	Diffusion-based	TSD-SR [86]	Diffusion-based
PiSA-SR [31]	Diffusion-based	ResShift [29]	Diffusion-based
SeeSR [32]	Diffusion-based	FLUX [87]	Generation
OSDiff [33]	Diffusion-based	Nano Banana [88]	Generation
CCSR [89]	Diffusion-based	BSRGAN [25]	GAN-based
DiffBIR [30]	Diffusion-based	CAL-GAN [26]	GAN-based
StableSR [4]	Diffusion-based	RealESRGAN [27]	GAN-based
PASD [34]	Diffusion-based	HAT [23]	PSNR-oriented
Invsr [90]	Diffusion-based	SwinIR [24]	PSNR-oriented

Table 1. Restoration or generation models used in the benchmark.

ous testsets is also rather limited. Most benchmarks adopt only a small set of simple degradations, with little deliberate design or diversity. This narrow coverage can be traced back to the weak generalization of earlier learning-based restoration models. Since these models rarely improved images corrupted by unfamiliar degradations, evaluating them on richer or more realistic degradation types was considered unnecessary or impractical [82, 83]. With the emergence of diffusion-based GIR models, this assumption no longer holds. Their strong content priors substantially enhance generalization and allow the model to recover natural content instead of merely removing specific corruptions [84]. Moreover, modern GIR models also exhibit highly nonuniform behavior across degradation types, performing well on some degradations while failing on others, making degradation-specific evaluation essential. To match this new capability, the evaluation protocol must also expand to include a broader and more realistic spectrum of degradations. We therefore construct a degradation suite that intentionally covers both synthetic and authentic real-world scenarios, as illustrated in Fig. 1. Our final dataset consists of two complementary components: a synthetic subset of 147 high-quality images across 21 semantic categories, degraded using the RealESRGAN [27] pipeline, and a real-world subset of 207 degraded images. Together, these components provide both semantic and degradation diversity, enabling a more comprehensive evaluation of GIR models.

3.2. Restoration Models Selection

In this work, we emphasize a comparative analysis of generative paradigms that prioritize perceptual quality in image restoration. To this end, we select 20 representative models spanning four distinct families, as listed in Tab. 1, which together generate 7,080 restored images on our test set. Rather than exhaustively surveying all methods, our selection captures the diverse design philosophies and generative behaviours exhibited across model families. Specifically, we include the following four categories. **(1) Diffusion-based models.** This group represents the current mainstream of GIR, leveraging diffusion processes to iteratively refine degraded inputs into high-quality outputs. These models include both those built upon large-scale pre-trained diffusion backbones (*e.g.*, Stable Diffusion or Flux) and

Dataset	# Images	# IR Model	# GIR Models	Multi. Aspect
SRIQA-Bench [9]	1.1K	10	8	✗
ISRGen-QA [8]	0.72K	15	10	✗
Ours	7K	20	18	✓

Table 2. Comparison of existing datasets for GIR assessment.

those trained from scratch specifically for restoration, differing mainly in whether their generative priors originate from external pretraining or task-specific supervision. **(2) General image generation models.** These models (*e.g.*, Nano Banana and Flux Kontext) perform image-to-image translation beyond conventional restoration pipelines, effectively blurring the boundary between image restoration and open-ended generation. **(3) GAN-based models.** Generative adversarial networks have long dominated perceptual image restoration before the diffusion era. Although their generative priors are generally weaker than those of diffusion-based models, they remain crucial baselines for comparison. **(4) PSNR-oriented models.** PSNR-oriented models achieve sharper edges and higher PSNR performance [10], representing restoration techniques trained under deterministic supervision. They rely less on generative priors and more on spatial-contextual modelling, providing a non-generative reference for evaluating realism-fidelity boundaries. These models demonstrate the evolving boundary between image restoration and general image generation, offering insight into how generative architectures behave in image restoration.

3.3. Design of the Human Evaluation

The goal of our human evaluation is not only to obtain an overall quality score for each restored image but also to understand why an image is perceived as good or bad. Unlike previous studies [8, 9] that rely solely on a single holistic score, our design introduces a multi-dimensional scoring framework that captures fine-grained perceptual and semantic aspects of generative restoration. This allows us to analyze specific failure sources and perceptual biases of different models. To achieve this, we identify the key perceptual dimensions most relevant to image restoration quality: Detail, Sharpness, Semantics, and Overall score.

Detail is scored on a bipolar scale from -3 to $+3$, capturing both under-generation and over-generation of details. Scores below 0 indicate insufficient or overly smoothed detail, while scores above 0 reflect excessive or hallucinated textures that deviate from natural appearance. 0 represents a perceptually balanced level of detail consistent with the input content. **Sharpness** is also evaluated on a -3 to $+3$ scale, measuring perceptual clarity. Negative scores correspond to blurry or poorly defined edges, whereas positive scores correspond to over-sharpened or haloed edges. 0 indicates appropriate, naturally sharp object boundaries. **Semantics** is assessed using a 0 to 4 scale, focusing on structural correctness and semantic alignment. 0 indicates complete semantic failure, which means the object is missing,

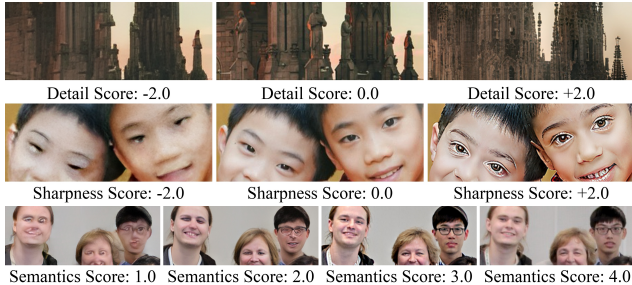


Figure 4. Illustration of our annotation criteria. The rows (top to bottom) indicate: Detail (under-generated [-2] to over-generated [+2]), Sharpness (blurred [-2] to over-sharpened [+2]), and Semantic correctness (severe failure [0] to fully consistent [4]).

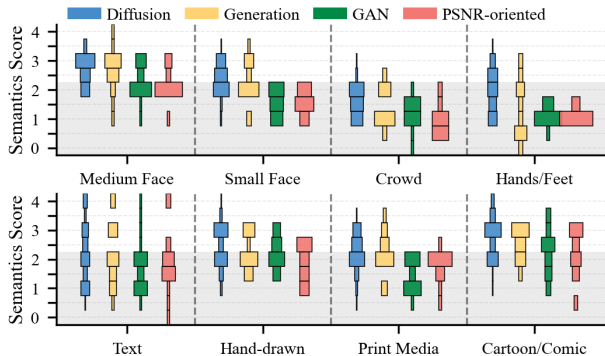


Figure 5. Distribution of semantic consistency scores across scenes. Box widths represent the sample percentage at each score. The light gray region marks unacceptable results.

replaced by irrelevant content, or entirely unrecognizable. 1 denotes an unsuccessful attempt at generating the intended semantics. At 2, the object is partly recognizable but exhibits some texture or geometric distortion. 3 corresponds to minor distortions with an overall recognizable and coherent structure. 4 represents a fully natural and semantically consistent restoration. **Overall** quality score reflects the evaluator’s willingness to accept the restoration as a final output, ranging from completely unacceptable 0 to fully satisfactory 4. Fig. 4 further illustrates representative examples corresponding to different score levels across the evaluated dimensions. A total of 56 human evaluators then scored these results following our defined evaluation dimensions and detailed rating criteria, enabling consistent and fine-grained perceptual assessment across models. Compared to previous datasets for generative restoration, our approach is significantly more comprehensive, as summarized in Tab. 2.

4. Results

4.1. Semantic-Dependent Behavior

Semantic specificity across all models. A key observation from Fig. 2 is that all restoration models exhibit highly uneven behavior across semantic categories. Different semantics pose inherently different levels of difficulty: some are consistently well restored, while others remain persistently challenging across all model families. This asymme-

try highlights that current restoration models are strongly influenced by the semantic content of the scene rather than degradation alone. It also suggests that model robustness is bounded not only by the type of degradation but also by the intrinsic structure and meaning of the visual content itself.

As shown in Fig. 2, most models perform well on *animal fur* and *cartoon/comic* semantics, with nearly all scores meeting or exceeding our acceptable threshold of 2. This indicates that models find it easier to consistently generate the textures typical of these categories. Meanwhile, semantics like *small faces*, *crowd*, *hands/feet*, *text* and *print media* remain difficult to restore, as shown in Fig. 6. Human perception is acutely sensitive to errors in both the structural coherence and semantic correctness of these particular categories. However, current models often fail to achieve this satisfactory level of realism, a limitation reflected in Fig. 2 where the majority of scores lie within the unacceptable region (shaded light gray). Their failures are evident in common artifacts such as distorted facial features, malformed hands, and illegible text, which do not align with human cognitive expectations and are consequently perceived as low-quality restorations.

Most restoration models still tend to under-generate fine details, resulting in overly smooth and textureless appearances, as shown in Fig. 3(a). While the overall distribution of detail scores is concentrated in the $[-2, -1]$ range. A closer look reveals a key difference between model families: we observe that GAN and PSNR-oriented models never over-generate details, whereas diffusion-based and generation methods possess a stronger capability for fine-grained synthesis, sometimes even to the point of over-generation. This architectural divergence marks a crucial turning point: while **current GIR models are clearly breaking the previous bottleneck of insufficient detail, they now face the new problem of over-generation**. Evaluating this emerging trade-off is precisely what underscores the necessity of our work in such fine-grained evaluation. This detail generation performance is also highly dependent on the semantic category. As illustrated in Fig. 3(a), models can generate abundant fine structures in scenes like *large faces* and *fabric texture*, but struggle with detail of *crowd* images.

We hypothesize two primary reasons for this phenomenon. First, despite their strong generative priors, existing models struggle to generalize fine-grained textures universally. Their priors are often biased towards common patterns, leading to inconsistent texture generation in geometrically complex or less-represented scenes. Second, aggressively generating detail risks introducing semantic or structural hallucinations. To mitigate this, modern diffusion-based approaches often adopt a conservative strategy, favoring smoother outputs that minimize artifacts. These observations highlight two kinds of difficulty in image restoration: The first comes from information deficiency in small,

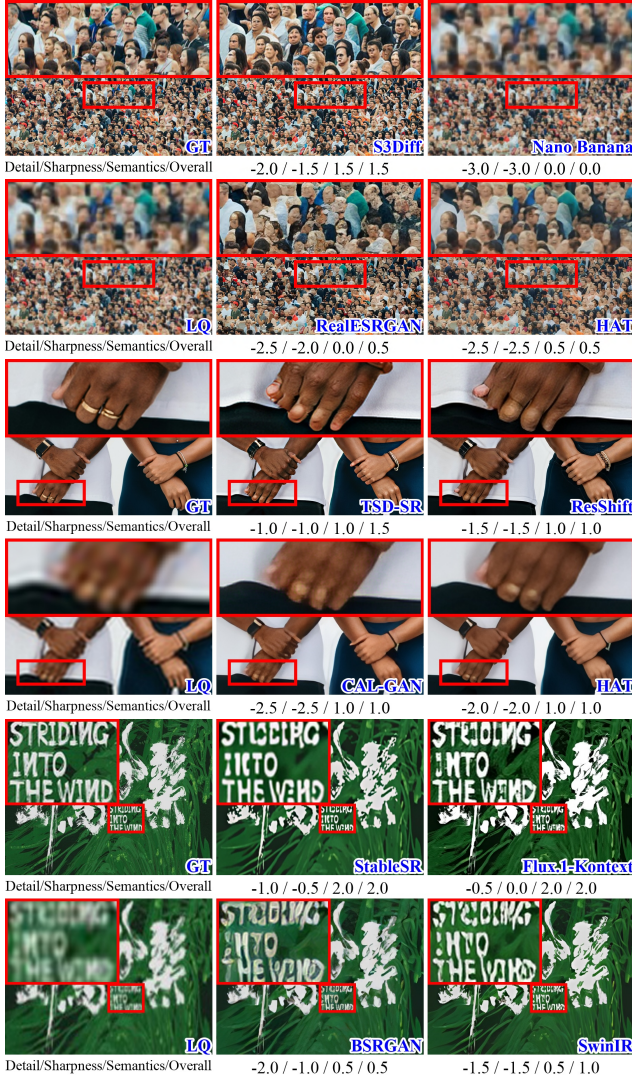


Figure 6. Common failure modes in hard cases: distorted faces in *crowd* scenes (top), structural errors in *hands/feet* (middle), and illegible characters in *text* (bottom).

low-resolution regions; The second arises from structural complexity in geometrically or semantically rich scenes. Moreover, humans are particularly sensitive to distortions in these high-level semantic regions, meaning that even subtle geometric or textual inconsistencies can drastically degrade perceived realism. This finding underscores the importance of semantically salient regions for evaluating restoration fidelity and perceptual plausibility.

Model family comparison. Overall, diffusion-based models achieve the highest upper-bound scores across nearly all semantic categories Fig. 2, demonstrating their promising potential in image restoration. This superior performance arises from their dual capability: they effectively remove low-level degradations while leveraging powerful generative priors to generate perceptually rich textures and details. As shown in Fig. 3, diffusion-based models are more likely to produce clearer and more detailed images, as their de-

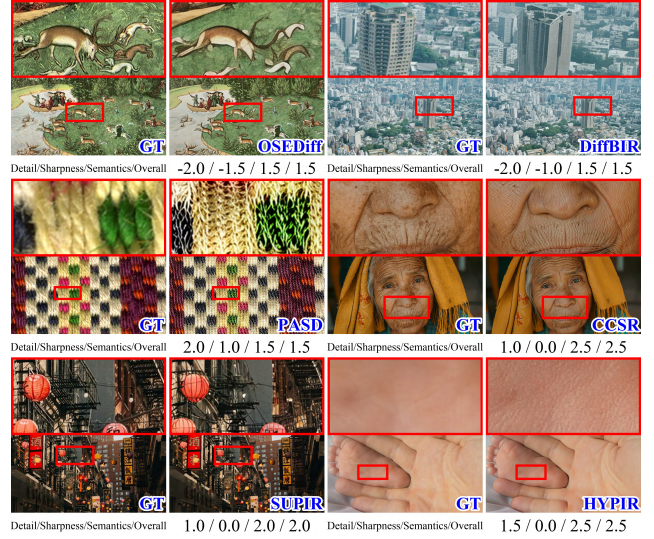


Figure 7. Diffusion models exhibit a dual tendency in detail generation: sometimes under-generating textures, leading to overly smooth results (top row), and at other times over-generating, creating implausible or redundant details (middle and bottom rows)



Figure 8. Examples illustrating over-generation, semantic infidelity, and degradation unremoval in generation models: more whiskers and railings are generated (first), the geometry of the face is not restored, and the position of the shoes is completely changed (second and third), and artifacts and noise are not eliminated (last).

tail scores are generally distributed closer to the balanced region (0 score) compared with other model families. However, diffusion-based models still have challenges in controlling their generative ability. On one hand, diffusion models may under-generate, producing smooth but visually incomplete restorations; on the other hand, they can easily over-generate, introducing excessive or unrealistic textures that deviate from the original input. As illustrated in Fig. 3(a), diffusion-based models may produce either insufficient or excessive details. In the *hand-drawn* example (top left), the model fails to generate enough fine-grained structures, resulting in flat textures. In texture-rich materials such as *fabric* (middle left), models tend to over-enhance local patterns, generating unnatural details. For *large face and hand/feet* scenes (middle right and bottom right), they frequently amplify surface textures and wrinkles beyond re-

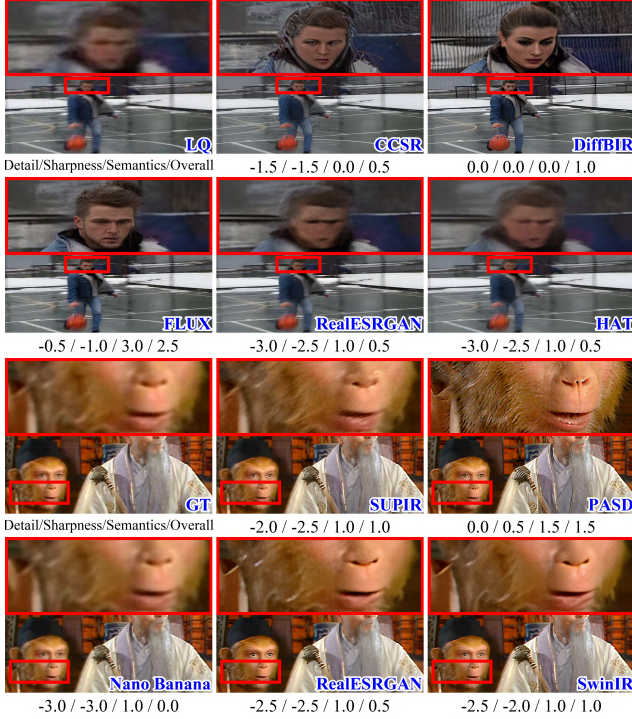


Figure 9. Examples of hard degradations (*motion blur*, *old film*).

alism, making the skin appear overly coarse. In *street view* (bottom left), the models over-generate fine structural elements such as lantern edges and railings, resulting in visually cluttered and chaotic line patterns. Furthermore, their semantic lower bounds remain comparable to those of other model families. As shown in Fig. 2, the performance of diffusion-based models also drops sharply in challenging scenes such as *crowd*, *hands/feet*, and *text*. Fig. 6 shows that in these scenes, diffusion-based models struggle to maintain geometric consistency and semantic coherence in such complex scenarios. Moreover, as shown in Fig. 3(a), excessive or exaggerated texture generation also undermines fidelity. This suggests that their performance limitations arise partly from the inherent difficulty of certain scenes, and partly from the challenge of controlling the generative process to produce details consistent with the input.

Generation models demonstrate limited robustness in image restoration. They sometimes match the overall score of diffusion-based models, yet the score fluctuates drastically across scenes. As shown in Figs. 2, 3 and 5, their upper bounds sometimes rival diffusion-based models, but their lower bounds drop sharply, revealing unstable restoration abilities and poor adaptability to diverse restoration conditions. This instability manifests in several ways. As illustrated in Fig. 3(a), generation models predominantly suffer from under-generation, often failing to produce sufficient fine details or restore complex textures. Occasionally, they exhibit an over-generating tendency, similar to diffusion-based models, as shown in the first example of Fig. 8. Generation models also suffer from semantic infidelity. Beyond

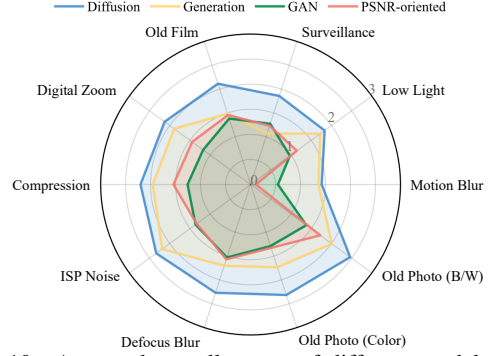


Figure 10. Averaged overall scores of different model families across various degradation types.

Config ID	Hands/ Feet	Aerial View	Config ID	Crowd	Street View	Config ID	Digital Zoom	OP (Color)
1	2.59	2.40	1	1.60	2.30	1	2.09	1.65
2	2.82	1.80	2	1.30	2.40	2	1.76	1.81

(a) DiffBIR

(b) PiSA-SR

(c) SUPIR

Table 3. Diffusion-based models’ parameter sensitivity. Mean scores show that the optimal configuration is scene- and degradation-dependent.

struggling to maintain geometric consistency and semantic coherence in difficult scenes, they sometimes alter the identity of the whole restored content, as shown in the second and third examples of Fig. 8. They further show limited ability to remove degradations: their sharpness scores remain low across many scenes, and the last examples of Fig. 8 reveal frequent residual blur and artifacts. These findings indicate that **simply applying general-purpose generative models to image restoration is insufficient**. Their lack of robustness and strong dependence on scene content highlight the need for the development of task-specific architectures.

PSNR-oriented and GAN-based approaches generally underperform diffusion-based models across most semantic categories and evaluation dimensions. As illustrated in Fig. 3(a), their upper-bound scores are lower than those of diffusion-based methods, reflecting limited generative capability and weaker texture generation. Fig. 3(b) shows that they exhibit an advantage in robustness over generation models. Their lower-bound scores are typically higher, suggesting a relatively reliable baseline.

4.2. Degradation-Dependent Behavior

Current restoration models still exhibit clear limitations when handling information-deficient degradations. In Fig. 10, degradation types such as *motion blur*, *old film*, *low light*, and *surveillance* exhibit noticeably lower average overall scores. Fig. 9 shows the restoration results of these degradations. These degradations remain challenging for existing GIR models. Their common characteristic lies in information loss and irreversible corruption: *motion blur* introduces overlapping spatial information; *surveillance* footage tends to be extremely low-resolution and

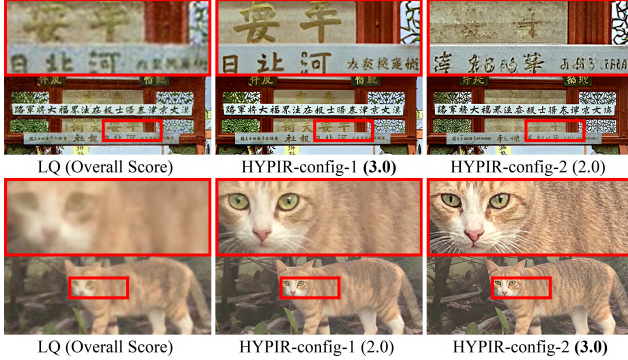


Figure 11. Effect of parameter configurations on restoration behavior in diffusion-based models (HYPIR as an example).

	NIQE	PI	MANIQA	MUSIQ	CLIP-IQA	DeQA-Score	Ours
SRCC	0.164	0.178	0.361	0.376	0.389	0.409	0.662
PLCC	0.206	0.230	0.391	0.427	0.420	0.464	0.677

Table 4. Performance comparison of existing IQA methods and our trained IQA model on our dataset.

Metric	Sharpness	Detail	Semantic	Total Score
SRCC / PLCC	0.633 / 0.645	0.575 / 0.603	0.585 / 0.622	0.662 / 0.677

Table 5. Performance on different aspects of our dataset.

blurry; *low-light* scenes provide limited visible cues; *old film* often suffers from extensive detail degradation. These degradations may require task-specific modeling beyond current general restoration frameworks.

Among all model families, diffusion-based models demonstrate relatively stronger robustness and generalization across different degradation types. As shown in Fig. 10, they achieve noticeably higher average overall scores than other architectures. However, their performance still drops in extreme cases, indicating that generative capability alone is insufficient when the input lacks recoverable information.

4.3. Sensitivity to Parameter Configuration

For diffusion-based models, parameter configuration proves to be a critical factor influencing restoration quality. As shown in Tab. 3, different parameter settings yield the highest overall scores in different semantic scenes and degradations. Fig. 11 further demonstrates diffusion-based models require scene- and degradation-specific parameter choices to achieve optimal restoration performance. While this sensitivity introduces additional complexity in model use, it also provides valuable flexibility: by properly tuning parameters, users can selectively emphasize realism or fidelity according to task requirements. Therefore, careful and context-aware parameter adjustment is essential to fully exploit the potential of diffusion-based models and achieve optimal restoration performance. To further enhance model usability and performance, we expect that future diffusion-based GIR frameworks should not only retain parameter-controllable flexibility but also incorporate adaptive mechanisms that automatically adjust generative strength based on scene semantics and degradation conditions.

5. Advances in Image Quality Assessment

Despite the rapid development of IQA techniques, existing methods [8–10] remain inadequate for evaluating the fine-grained behaviors of GIR models. Conventional IQA metrics are limited in two key aspects. First, they often fail to produce accurate predictions in semantically inconsistent cases, especially when the restored image deviates from the original semantic details. Second, most IQA models provide only a single score, which cannot capture the multi-dimensional nature of GIR quality, where sharpness, detail, semantics, and overall score may vary independently.

Our work represents the first effort to perform multi-dimensional, fine-grained analysis of GIR models. Leveraging our human-annotated dataset, which provides scores along multiple dimensions, we train an IQA model capable of both holistic and dimension-specific quality prediction. This enables diagnostic evaluation of restored images that existing single-score IQA frameworks cannot provide. We thus split our dataset by 9:1 for training and evaluation, then train a baseline IQA model using the DeQA-Score framework [73]. We use Spearman Rank Correlation Coefficient (SRCC) and Pearson Linear Correlation Coefficient (PLCC) to measure alignment with human annotations.

We compare our IQA model with leading no-reference methods (NIQE [50], PI [91], MANIQA [66], MUSIQ [65], CLIP-IQA [71], DeQA-Score [73]) on our dataset, which is specifically designed to challenge models with diverse semantics and degradations. As shown in Tab. 4, the inability of existing methods to generalize to these conditions is evident in their poor performance. In contrast, our model achieves SRCC of **0.662** and PLCC of **0.677**. We also evaluate the IQA models trained on each dimension in Tab. 5. The experimental results demonstrate that conventional IQA methods are insufficient for analyzing the complex behaviors of modern GIR models. Our trained IQA framework, grounded in fine-grained perceptual and semantic annotations, allows not only accurate overall quality prediction but also interpretable diagnosis of specific aspects. This multi-dimensional approach provides a new foundation for perceptually aligned evaluation and could guide the development of next-generation restoration metrics and intelligent evaluation agents.

6. Conclusion

In this work, we present the first fine-grained framework for understanding GIR across both semantic scenes and degradation types. By constructing a carefully balanced test set, introducing multi-dimensional human annotations, and analyzing 20 representative models, we reveal the strengths and limitations of modern GIR systems. We hope this work provides a foundation for more reliable GIR evaluation and inspires future research toward controllable, robust, and semantically faithful restoration models.

References

- [1] Christian Ledig, Lucas Theis, Ferenc Huszár, Jose Caballero, Andrew Cunningham, Alejandro Acosta, Andrew Aitken, Alykhan Tejani, Johannes Totz, Zehan Wang, et al. Photo-realistic single image super-resolution using a generative adversarial network. In *CVPR*, 2017. 1
- [2] Xintao Wang, Ke Yu, Shixiang Wu, Jinjin Gu, Yihao Liu, Chao Dong, Yu Qiao, and Chen Change Loy. Esrgan: Enhanced super-resolution generative adversarial networks. In *ECCV*, 2018. 2
- [3] Chitwan Saharia, Jonathan Ho, William Chan, Tim Salimans, David J Fleet, and Mohammad Norouzi. Image super-resolution via iterative refinement. *IEEE TPAMI*, 2022.
- [4] Jianyi Wang, Zongsheng Yue, Shangchen Zhou, Kelvin CK Chan, and Chen Change Loy. Exploiting diffusion prior for real-world image super-resolution. *IJCV*, 2024. 4
- [5] Fanghua Yu, Jinjin Gu, Zheyuan Li, Jinfan Hu, Xiangtao Kong, Xintao Wang, Jingwen He, Yu Qiao, and Chao Dong. Scaling up to excellence: Practicing model scaling for photo-realistic image restoration in the wild. In *CVPR*, 2024. 2, 4
- [6] Xinqi Lin, Fanghua Yu, Jinfan Hu, Zhiyuan You, Wu Shi, Jimmy S Ren, Jinjin Gu, and Chao Dong. Harnessing diffusion-yielded score priors for image restoration. In *SIGGRAPH Asia*, 2025. 1, 2, 4
- [7] Xin Li, Yulin Ren, Xin Jin, Cuiling Lan, Xingrui Wang, Wenjun Zeng, Xinchao Wang, and Zhibo Chen. Diffusion models for image restoration and enhancement: a comprehensive survey. *IJCV*, 2025. 1, 2
- [8] Yixiao Li, Xin Li, Chris Wei Zhou, Shuo Xing, Hadi Amirpour, Xiaoshuai Hao, Guanghui Yue, Baoquan Zhao, Weide Liu, Xiaoyuan Yang, et al. VQualA 2025 challenge on image super-resolution generated content quality assessment: Methods and results. In *CVPR Workshops*, 2025. 2, 3, 4, 8
- [9] Du Chen, Tianhe Wu, Kede Ma, and Lei Zhang. Toward generalized image quality assessment: Relaxing the perfect reference quality assumption. In *CVPR*, 2025. 2, 3, 4
- [10] Ekta Prashnani, Hong Cai, Yasamin Mostofi, and Pradeep Sen. PieAPP: Perceptual image-error assessment through pairwise preference. In *CVPR*, 2018. 2, 4, 8
- [11] Gu Jinjin, Cai Haoming, Chen Haoyu, Ye Xiaoxing, Jimmy S Ren, and Dong Chao. PIPAL: a large-scale image quality assessment dataset for perceptual image restoration. In *ECCV*, 2020. 2
- [12] Kai Zhang, Wangmeng Zuo, Yunjin Chen, Deyu Meng, and Lei Zhang. Beyond a gaussian denoiser: Residual learning of deep cnn for image denoising. *IEEE TIP*, 2017. 2
- [13] Haoyu Chen, Jinjin Gu, Yihao Liu, Salma Abdel Magid, Chao Dong, Qiong Wang, Hanspeter Pfister, and Lei Zhu. Masked image training for generalizable deep image denoising. In *CVPR*, 2023.
- [14] Diego Valsesia, Giulia Fracastoro, and Enrico Magli. Deep graph-convolutional image denoising. *IEEE TIP*, 2020. 2
- [15] Seungjun Nah, Tae Hyun Kim, and Kyoung Mu Lee. Deep multi-scale convolutional neural network for dynamic scene deblurring. In *CVPR*, 2017. 2
- [16] Zheng Chen, Yulun Zhang, Ding Liu, Jinjin Gu, Linghe Kong, Xin Yuan, et al. Hierarchical integration diffusion model for realistic image deblurring. In *NeurIPS*, 2023.
- [17] Orest Kupyn, Volodymyr Budzan, Mykola Mykhailych, Dmytro Mishkin, and Jiří Matas. Deblurgan: Blind motion deblurring using conditional adversarial networks. In *CVPR*, 2018. 2
- [18] Xueyang Fu, Jiabin Huang, Xinghao Ding, Yinghao Liao, and John Paisley. Clearing the skies: A deep network architecture for single-image rain removal. *IEEE TIP*, 2017. 2
- [19] Jinjin Gu, Xianzheng Ma, Xiangtao Kong, Yu Qiao, and Chao Dong. Networks are slacking off: Understanding generalization problem in image deraining. In *NeurIPS*, 2023. 2
- [20] Chao Dong, Chen Change Loy, Kaiming He, and Xiaoou Tang. Learning a deep convolutional network for image super-resolution. In *ECCV*, 2014. 2
- [21] Tao Dai, Jianrui Cai, Yongbing Zhang, Shu-Tao Xia, and Lei Zhang. Second-order attention network for single image super-resolution. In *CVPR*, 2019.
- [22] Bee Lim, Sanghyun Son, Heewon Kim, Seungjun Nah, and Kyoung Mu Lee. Enhanced deep residual networks for single image super-resolution. In *CVPR Workshops*, 2017.
- [23] Xiangyu Chen, Xintao Wang, Jiantao Zhou, Yu Qiao, and Chao Dong. Activating more pixels in image super-resolution transformer. In *CVPR*, 2023. 4
- [24] Jingyun Liang, Jie Zhang Cao, Guolei Sun, Kai Zhang, Luc Van Gool, and Radu Timofte. Swinir: Image restoration using swin transformer. In *ICCV*, 2021. 2, 4
- [25] Kai Zhang, Jingyun Liang, Luc Van Gool, and Radu Timofte. Designing a practical degradation model for deep blind image super-resolution. In *ICCV*, 2021. 2, 4
- [26] Joonkyu Park, Sanghyun Son, and Kyoung Mu Lee. Content-aware local gan for photo-realistic super-resolution. In *ICCV*, 2023. 4
- [27] Xintao Wang, Liangbin Xie, Chao Dong, and Ying Shan. Real-ESRGAN: Training real-world blind super-resolution with pure synthetic data. In *ICCV Workshops*, 2021. 2, 4, 13
- [28] Ziwei Luo, Fredrik K Gustafsson, Zheng Zhao, Jens Sjölund, and Thomas B Schön. Refusion: Enabling large-size realistic image restoration with latent-space diffusion models. In *CVPR*, 2023. 2
- [29] Zongsheng Yue, Jianyi Wang, and Chen Change Loy. Resshift: Efficient diffusion model for image super-resolution by residual shifting. In *NeurIPS*, 2023. 2, 4
- [30] Xinqi Lin, Jingwen He, Ziyang Chen, Zhaoyang Lyu, Bo Dai, Fanghua Yu, Yu Qiao, Wanli Ouyang, and Chao Dong. Diffbir: Toward blind image restoration with generative diffusion prior. In *ECCV*, 2024. 2, 4
- [31] Lingchen Sun, Rongyuan Wu, Zhiyuan Ma, Shuaizheng Liu, Qiaosi Yi, and Lei Zhang. Pixel-level and semantic-level adjustable super-resolution: A dual-lora approach. In *CVPR*, 2025. 4
- [32] Rongyuan Wu, Tao Yang, Lingchen Sun, Zhengqiang Zhang, Shuai Li, and Lei Zhang. Seesr: Towards semantics-

- aware real-world image super-resolution. In *CVPR*, 2024. 4
- [33] Rongyuan Wu, Lingchen Sun, Zhiyuan Ma, and Lei Zhang. One-step effective diffusion network for real-world image super-resolution. In *NeurIPS*, 2024. 4
- [34] Tao Yang, Rongyuan Wu, Peiran Ren, Xuansong Xie, and Lei Zhang. Pixel-aware stable diffusion for realistic image super-resolution and personalized stylization. In *ECCV*, 2024. 2, 4
- [35] Zhou Wang, Alan C Bovik, Hamid R Sheikh, and Eero P Simoncelli. Image quality assessment: from error visibility to structural similarity. *IEEE TIP*, 2004. 2
- [36] Lin Zhang, Lei Zhang, Xuanqin Mou, and David Zhang. FSIM: A feature similarity index for image quality assessment. *IEEE TIP*, 2011. 2
- [37] Hamid R Sheikh and Alan C Bovik. Image information and visual quality. *IEEE TIP*, 2006. 2
- [38] Richard Zhang, Phillip Isola, Alexei A Efros, Eli Shechtman, and Oliver Wang. The unreasonable effectiveness of deep features as a perceptual metric. In *CVPR*, 2018. 2
- [39] Hanhe Lin, Vlad Hosu, and Dietmar Saupe. KADID-10K: A large-scale artificially distorted iqa database. In *International Conference on Quality of Multimedia Experience (QoMEX)*, 2019. 2
- [40] H Sheikh. LIVE image quality assessment database release 2. <http://live.ece.utexas.edu/research/quality>, 2005. 2
- [41] Sebastian Bosse, Dominique Maniry, Klaus-Robert Müller, Thomas Wiegand, and Wojciech Samek. Deep neural networks for no-reference and full-reference image quality assessment. *IEEE TIP*, 2018. 2
- [42] Yue Cao, Zhaolin Wan, Dongwei Ren, Zifei Yan, and Wangmeng Zuo. Incorporating semi-supervised and positive-unlabeled learning for boosting full reference image quality assessment. In *CVPR*, 2022.
- [43] Keyan Ding, Kede Ma, Shiqi Wang, and Eero P Simoncelli. Image quality assessment: Unifying structure and texture similarity. *IEEE TPAMI*, 2020.
- [44] Keyan Ding, Yi Liu, Xueyi Zou, Shiqi Wang, and Kede Ma. Locally adaptive structure and texture similarity for image quality assessment. In *ACM MM*, 2021.
- [45] Abhijay Ghildyal and Feng Liu. Shift-tolerant perceptual similarity metric. In *ECCV*, 2022.
- [46] Guanghao Yin, Wei Wang, Zehuan Yuan, Chuchu Han, Wei Ji, Shouqian Sun, and Changhu Wang. Content-variant reference image quality assessment via knowledge distillation. In *AAAI*, 2022.
- [47] Wei Zhou and Zhou Wang. Quality assessment of image super-resolution: Balancing deterministic and statistical fidelity. In *ACM MM*, 2022. 2
- [48] Chao Ma, Chih-Yuan Yang, Xiaokang Yang, and Ming-Hsuan Yang. Learning a no-reference quality metric for single-image super-resolution. *Computer Vision and Image Understanding*, 2017. 2
- [49] Anish Mittal, Anush Krishna Moorthy, and Alan Conrad Bovik. No-reference image quality assessment in the spatial domain. *IEEE TIP*, 2012.
- [50] Anish Mittal, Rajiv Soundararajan, and Alan C Bovik. Making a “completely blind” image quality analyzer. *IEEE Sign. Process. Letters*, 2012. 8
- [51] Anush Krishna Moorthy and Alan Conrad Bovik. A two-step framework for constructing blind image quality indices. *IEEE Sign. Process. Letters*, 2010.
- [52] Anush Krishna Moorthy and Alan Conrad Bovik. Blind image quality assessment: From natural scene statistics to perceptual quality. *IEEE TIP*, 2011.
- [53] Michele A Saad, Alan C Bovik, and Christophe Charrier. Blind image quality assessment: A natural scene statistics approach in the dct domain. *IEEE TIP*, 2012.
- [54] Huixuan Tang, Neel Joshi, and Ashish Kapoor. Learning a blind measure of perceptual image quality. In *CVPR*, 2011. 2
- [55] Le Kang, Peng Ye, Yi Li, and David Doermann. Convolutional neural networks for no-reference image quality assessment. In *CVPR*, 2014. 2
- [56] Xialei Liu, Joost van de Weijer, and Andrew D. Bagdanov. RankIQA: Learning from rankings for no-reference image quality assessment. In *ICCV*, 2017.
- [57] Da Pan, Ping Shi, Ming Hou, Zefeng Ying, Sizhe Fu, and Yuan Zhang. Blind predicting similar quality map for image quality assessment. In *CVPR*, 2018.
- [58] Shaolin Su, Qingsen Yan, Yu Zhu, Cheng Zhang, Xin Ge, Jinqiu Sun, and Yanning Zhang. Blindly assess image quality in the wild guided by a self-adaptive hyper network. In *CVPR*, 2020.
- [59] Simen Sun, Tao Yu, Jiahua Xu, Wei Zhou, and Zhibo Chen. GraphIQA: Learning distortion graph representations for blind image quality assessment. *IEEE TMM*, 2022.
- [60] Heliang Zheng, Jianlong Fu, Yanhong Zeng, Zheng-Jun Zha, and Jiebo Luo. Learning conditional knowledge distillation for degraded-reference image quality assessment. *ICCV*, 2021.
- [61] Hancheng Zhu, Leida Li, Jinjian Wu, Weisheng Dong, and Guangming Shi. MetaIQA: deep meta-learning for no-reference image quality assessment. In *CVPR*, 2020.
- [62] Weixia Zhang, Dingquan Li, Chao Ma, Guangtao Zhai, Xiaokang Yang, and Kede Ma. Continual learning for blind image quality assessment. *IEEE TPAMI*, 2022.
- [63] Zhenqiang Ying, Haoran Niu, Praful Gupta, Dhruv Mahajan, Deepti Ghadiyaram, and Alan Bovik. From patches to pictures (PaQ-2-PiQ): Mapping the perceptual space of picture quality. In *CVPR*, 2020.
- [64] Weixia Zhang, Kede Ma, Guangtao Zhai, and Xiaokang Yang. Uncertainty-aware blind image quality assessment in the laboratory and wild. *IEEE TIP*, 2021.
- [65] Junjie Ke, Qifei Wang, Yilin Wang, Peyman Milanfar, and Feng Yang. MUSIQ: Multi-scale image quality transformer. In *CVPR*, 2021. 8
- [66] Sidi Yang, Tianhe Wu, Shuwei Shi, Shanshan Lao, Yuan Gong, Mingdeng Cao, Jiahao Wang, and Yujiu Yang. MANIQA: Multi-dimension attention network for no-reference image quality assessment. In *CVPR Workshops*, 2022. 8

- [67] Weixia Zhang, Guangtao Zhai, Ying Wei, Xiaokang Yang, and Kede Ma. Blind image quality assessment via vision-language correspondence: A multitask learning perspective. In *CVPR*, 2023. 2
- [68] Vlad Hosu, Hanhe Lin, Tamas Sziranyi, and Dietmar Saupe. KonIQ-10K: An ecologically valid database for deep learning of blind image quality assessment. *IEEE TIP*, 2020. 2
- [69] Yuming Fang, Hanwei Zhu, Yan Zeng, Kede Ma, and Zhou Wang. Perceptual quality assessment of smartphone photography. In *CVPR*, 2020.
- [70] Chunyi Li, Zicheng Zhang, Haoning Wu, Wei Sun, Xiongkuo Min, Xiaohong Liu, Guangtao Zhai, and Weisi Lin. AGIQA-3K: An open database for ai-generated image quality assessment. *IEEE TCSVT*, 2023. 2
- [71] Jianyi Wang, Kelvin CK Chan, and Chen Change Loy. Exploring clip for assessing the look and feel of images. In *AAAI*, 2023. 2, 8
- [72] Haoning Wu, Zicheng Zhang, Weixia Zhang, Chaofeng Chen, Chunyi Li, Liang Liao, Annan Wang, Erli Zhang, Wenxiu Sun, Qiong Yan, Xiongkuo Min, Guangtai Zhai, and Weisi Lin. Q-Align: Teaching LMMs for visual scoring via discrete text-defined levels. In *ICML*, 2024.
- [73] Zhiyuan You, Xin Cai, Jinjin Gu, Tianfan Xue, and Chao Dong. Teaching large language models to regress accurate image quality scores using score distribution. In *CVPR*, 2025. 8, 16
- [74] Zhiyuan You, Zheyuan Li, Jinjin Gu, Zhenfei Yin, Tianfan Xue, and Chao Dong. Depicting beyond scores: Advancing image quality assessment through multi-modal language models. In *ECCV*, 2024.
- [75] Zhiyuan You, Jinjin Gu, Zheyuan Li, Xin Cai, Kaiwen Zhu, Chao Dong, and Tianfan Xue. Descriptive image quality assessment in the wild. *arXiv preprint arXiv:2405.18842*, 2024.
- [76] Weiqi Li, Xuanyu Zhang, Shijie Zhao, Yabin Zhang, Junlin Li, Li Zhang, and Jian Zhang. Q-Insight: Understanding image quality via visual reinforcement learning. In *NeurIPS*, 2025.
- [77] Tianhe Wu, Jian Zou, Jie Liang, Lei Zhang, and Kede Ma. Visualquality-r1: Reasoning-induced image quality assessment via reinforcement learning to rank. In *NeurIPS*, 2025. 2
- [78] Xiangfei Sheng, Xiaofeng Pan, Zhichao Yang, Pengfei Chen, and Leida Li. Fine-grained image quality assessment for perceptual image restoration. *arXiv preprint arXiv:2508.14475*, 2025. 2
- [79] Jinglin Chen, Yongming Huang, Tianhao Lv, et al. TextDiffuser: Diffusion models as text painters. In *NeurIPS*, 2023. 3
- [80] Hao Zhang, Bo Zhu, Yuhang Cao, et al. Hand1000: Generating realistic hands from text with only 1,000 images. In *AAAI*, 2025.
- [81] Guo Liang, Qiang Fan, Bo Fu, et al. AuthFace: Towards authentic blind face restoration with face-oriented generative diffusion prior. In *ACM MM*, 2025. 3
- [82] Jinfan Hu, Jinjin Gu, Shiyao Yu, Fanghua Yu, Zheyuan Li, Zhiyuan You, Chaochao Lu, and Chao Dong. Interpreting low-level vision models with causal effect maps. *IEEE TPAMI*, 47(8):6396–6409, 2025. 4
- [83] Yihao Liu, Anran Liu, Jinjin Gu, Zhipeng Zhang, Wenhao Wu, Yu Qiao, and Chao Dong. Discovering distinctive "semantics" in super-resolution networks. *arXiv preprint arXiv:2108.00406*, 2021. 4
- [84] Jinfan Hu, Zhiyuan You, Jinjin Gu, Kaiwen Zhu, Tianfan Xue, and Chao Dong. Revisiting the generalization problem of low-level vision models through the lens of image deraining. *arXiv preprint arXiv:2502.12600*, 2025. 4
- [85] Aiping Zhang, Zongsheng Yue, Renjing Pei, Wenqi Ren, and Xiaochun Cao. Degradation-guided one-step image super-resolution with diffusion priors. *arXiv preprint arXiv:2409.17058*, 2024. 4
- [86] Linwei Dong, Qingnan Fan, Yihong Guo, Zhonghao Wang, Qi Zhang, Jinwei Chen, Yawei Luo, and Changqing Zou. Tsd-sr: One-step diffusion with target score distillation for real-world image super-resolution. In *CVPR*, 2025. 4
- [87] Stephen Batifol, Andreas Blattmann, Frederic Boesel, Saksham Consul, Cyril Diagne, Tim Dockhorn, Jack English, Zion English, Patrick Esser, Sumith Kulal, et al. FLUX.1 Kontext: Flow matching for in-context image generation and editing in latent space. *arXiv preprint arXiv:2506.15742*, 2025. 4
- [88] Google. Gemini 2.5 flash image (Nano Banana), 2025. 4
- [89] Lingchen Sun, Rongyuan Wu, Jie Liang, Zhengqiang Zhang, Hongwei Yong, and Lei Zhang. Improving the stability and efficiency of diffusion models for content consistent super-resolution. *arXiv preprint arXiv:2401.00877*, 2023. 4
- [90] Zongsheng Yue, Kang Liao, and Chen Change Loy. Arbitrary-steps image super-resolution via diffusion inversion. In *CVPR*, 2025. 4
- [91] Yochai Blau and Tomer Michaeli. The perception-distortion tradeoff. In *CVPR*, 2018. 8
- [92] Wikimedia Commons. Wikimedia commons: a collection of 129,990,166 freely usable media files to which anyone can contribute. 13
- [93] Unsplash. Unsplash: Beautiful free images & pictures.
- [94] Pixabay. Pixabay: Beautiful free images & royalty free stock.
- [95] International Photography Magazine & Grant. International photography magazine. 13
- [96] Hajime Nada, Vishwanath Sindagi, He Zhang, and Vishal M Patel. Pushing the limits of unconstrained face detection: a challenge dataset and baseline results. *arXiv preprint arXiv:1804.10275*, 2018. 13
- [97] Josue Anaya and Adrian Barbu. Renoir—a dataset for real low-light image noise reduction. *Journal of Visual Communication and Image Representation*, 2018.
- [98] Junyong Lee, Hyeonseok Son, Jaesung Rim, Sunghyun Cho, and Seungyong Lee. Iterative filter adaptive network for single image defocus deblurring. In *CVPR*, 2021.
- [99] Jianping Shi, Li Xu, and Jiaya Jia. Discriminative blur detection features. In *CVPR*, 2014.

- [100] Abdullah Abuolaim and Michael S Brown. Defocus deblurring using dual-pixel data. In *ECCV*, 2020.
- [101] Jie Liang, Radu Timofte, Qiaosi Yi, Zhengqiang Zhang, Shuaizheng Liu, Lingchen Sun, Rongyuan Wu, Xindong Zhang, Hui Zeng, Lei Zhang, et al. Ntire 2025 the 2nd restore any image model (raim) in the wild challenge. In *CVPR Workshops*, 2025.
- [102] Aashish Sharma and Robby T Tan. Nighttime visibility enhancement by increasing the dynamic range and suppression of light effects. In *CVPR*, 2021.
- [103] Eirikur Agustsson and Radu Timofte. NTIRE 2017 challenge on single image super-resolution: Dataset and study. In *CVPR Workshops*, 2017.
- [104] Jia-Bin Huang, Abhishek Singh, and Narendra Ahuja. Single image super-resolution from transformed self-exemplars. In *CVPR*, 2015.
- [105] Aoxiang Ning, Minglong Xue, Yiting Wei, Mingliang Zhou, and Senming Zhong. Artistic-style text detector and a new movie-poster dataset. *Expert Systems with Applications*, 2025.
- [106] Xin Yu, Peng Dai, Wenbo Li, Lan Ma, Jiajun Shen, Jia Li, and Xiaojuan Qi. Towards efficient and scale-robust ultra-high-definition image demoiréing. In *ECCV*, 2022.
- [107] Babak Saleh and Ahmed Elgammal. Large-scale classification of fine-art paintings: Learning the right metric on the right feature. *arXiv preprint arXiv:1505.00855*, 2015.
- [108] Yalong Bai, Yuxiang Chen, Wei Yu, Linfang Wang, and Wei Zhang. Products-10k: A large-scale product recognition dataset. *arXiv preprint arXiv:2008.10545*, 2020.
- [109] Waqas Sultani, Chen Chen, and Mubarak Shah. Real-world anomaly detection in surveillance videos. In *CVPR*, 2018. [13](#)
- [110] Andrew F Hayes and Klaus Krippendorff. Answering the call for a standard reliability measure for coding data. *Communication methods and measures*, 1(1):77–89, 2007. [15](#)

How Far Have We Gone in Generative Image Restoration?

A Study on its Capability, Limitations and Evaluation Practices

Supplementary Material

Appendix

This Appendix provides additional details, quantitative and qualitative results that complement the findings presented in the main paper. It is organized as follows: Appendix A provides comprehensive details of our dataset construction and implementation details of GIR models. Appendix B shows additional score distributions across semantic scenes and degradation types. The section also reports extended quantitative and qualitative results for parameter sensitivity analysis. Appendix C presents qualitative demonstrations of the limitations of existing IQA methods. Appendix D provides additional failure cases of current GIR models. Appendix E reports detailed per-model performance across all evaluation dimensions. Appendix F provides training details and more qualitative results of our IQA model.

A. Details of Evaluation Design

A.1. Details of the dataset

The images in dataset are collected from both open-access online repositories [92–95], our own captured photographs and existing degradation datasets [96–109]. Together, these sources provide rich semantic diversity and a broad range of real-world degradations, providing a solid foundation for evaluating the behavior of GIR models under different conditions.

All images are processed to a unified resolution of 1024×1024 . Each restoration model receives a 1024×1024 degraded image as input and produces a restored output of the same resolution, ensuring consistent comparison across all GIR models.

For the synthetic subset of 147 high-quality images across 21 semantic categories, we apply degradations using the official RealESRGAN pipeline [27]. The two-stage degradation framework of Real-ESRGAN can span an extremely severe degradation space, so severe that the entire image becomes unrecognizable to humans. This goes beyond realistic image degradation and loses practical meaning for restoration. To ensure that input images remain meaningful for evaluation, we have made several modifications to the default degradation settings. We fix the blur kernel size to 17×17 for both stages and constrain the blur standard deviations to $[0.2, 1.5]$ and $[0.2, 0.8]$ respectively. The probability of applying the final sinc filter is reduced from 0.8 to 0.4. In both degradation stages, only Gaussian noise is added, with noise levels set to $[1, 10]$ in stage 1 and $[1, 5]$ in stage 2. The resize operation is applied within

scale ranges of $[0.5, 1.5]$ in stage 1 and $[0.8, 1.2]$ in stage 2. JPEG compression levels are restricted to $[50, 95]$ and $[60, 95]$, producing moderate compression artifacts compared with the original broader ranges. Overall, these adjustments intentionally lighten the default RealESRGAN degradation strength, allowing us to introduce diverse but not overly destructive degradations. This ensures that the synthetic inputs remain realistic and challenging while still preserving enough visual information for meaningful generative restoration.

To better demonstrate the semantic and degradation diversity covered in our benchmark, we include extended visual examples in Figs. 13 to 16.

A.2. Implementation Details of Restoration Models

Most models were evaluated using their official default configurations, including pretrained weights and recommended inference hyperparameters, to ensure fair comparison and reproducibility. For SUPIR, we adopt the configuration `s_stage2 = 0.85`, `s_cfg = 4.0`, `spt_linear_CFG = 1.0`, and `s_noise = 1.007`. For HYPIR, we use the Flux-based variant and set `sharpness = 800` and `noise = 200`, without any prompt provided. For PASD, we evaluate the model using its official SD-XL version.

Generation models require prompts for image-to-image restoration. To ensure consistency, we use the same prompt across both generation models:

```
Perform high-quality image
restoration and super-resolution
in this image: enhance clar-
ity, remove noise and scratches,
reduce blur, and sharpen fine
details, while preserving a nat-
ural, realistic appearance with-
out over-processing or artifi-
cial artifacts.
```

To verify that our choice of prompt does not bias the evaluation, we further tested each generation model using several alternative prompts. Across all tested prompts, we observed only minor variations in overall perceptual quality and no systematic improvement over the main prompt we used. Representative comparisons of different prompts are shown in the Figs. 17 and 18, demonstrating that our chosen prompt provides stable and representative restoration behavior.

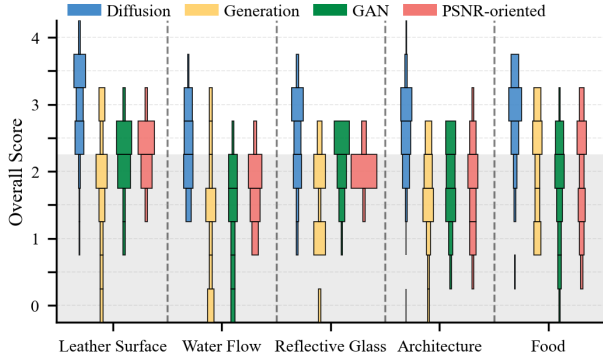


Figure 12. Distribution of annotated overall scores across semantic scene groups. The horizontal width of each box indicates the percentage of samples within each score interval. The light gray region indicates low overall scores, representing generally unacceptable results.

A.3. Detailed Criteria of Human Evaluation

Here, we provide the full detailed criteria used by annotators during manual evaluation, expanding upon the definitions of **Detail**, **Sharpness**, and **Semantics**.

Detail. This dimension evaluates the amount of fine-grained textures. -3: The restored image exhibits almost no improvement in local or global detail. Fine patterns, textures, or surface structures are largely absent, and most objects appear flat and featureless. -2: The restoration introduces limited additional detail compared to the degraded input. Fine textures and local variations remain largely missing or underdeveloped. -1: The image shows moderate enhancement in detail, but fine textures are still partially missing or over-smoothed in certain regions. 0: The level of detail is appropriate and consistent with the content of the input image. Textures are well-balanced, yielding a natural and realistic appearance. 1: Additional details beyond the original content are generated. These details slightly deviate from the ground truth and reduce overall realism. 2: A considerable amount of excessive or inconsistent detail is introduced, producing cluttered textures or unnatural structures that degrade visual authenticity. 3: The restoration introduces an overwhelming number of artificial and incoherent details, leading to an overly complex, chaotic, and unrealistic appearance.

Sharpness. -3: The restored image remains as blurry as the low-quality input, showing no perceptual improvement in clarity. -2: The image shows a slight overall improvement in clarity but remains noticeably blurry across most regions. -1: The image appears generally clear, yet minor blurriness persists in specific local regions. 0: Sharpness is appropriate; object boundaries appear clear, continuous, and natural. 1: Object boundaries are slightly sharper than

Model	Config ID	Configurations
HYPIR	1	sharpness:800, noise:600
	2	sharpness:4000, noise:200
	3	sharpness:4000, noise:600
PiSA-SR	1	lambda_pix:1.0, lambda_sem:0.3
	2	lambda_pix:2.0, lambda_sem:1.0
	3	lambda_pix:0.3, lambda_sem:1.0
SeeSR	1	conditioning_scale:1.0
	2	conditioning_scale:1.5
	3	conditioning_scale:2.0
DiffBIR	1	cfg_scale:1, noise_aug:0
	2	cfg_scale:10, noise_aug:0
	3	cfg_scale:1, noise_aug:5
	4	cfg_scale:10, noise_aug:5
SUPIR	1	s_stage2:1.0, s_noise:1.030 s_cfg:6.5, spt_linear_CFG:3.5
	2	s_stage2:0.7, s_noise:1.030 s_cfg:6.5, spt_linear_CFG:3.5
	3	s_stage2:0.58, s_noise:1.007 s_cfg:4.0, spt_linear_CFG:1.0
	4	s_stage2:1.0, s_noise:1.007 s_cfg:4.0, spt_linear_CFG:1.0

Table 6. Configurations used in our parameter sensitivity analysis. All other parameters remain at their official defaults.

those in natural scenes. The excessive edge enhancement slightly degrades perceptual quality. 2: Object boundaries appear overly sharp and unnatural, sometimes producing artifacts such as white halos or excessive contrast. 3: The entire image appears excessively sharp and highly unnatural, with very strong white edges and exaggerated contrast.

Semantics. 0: Total absence of the required category’s semantics. Object completely missing, unrecognizable, or the content is pure hallucination relative to the input. 1: Semantic generation was attempted but resulted in a highly chaotic structure, making the intended object unidentifiable or leading to critical structural failure. 2: Semantic structure is recognizable, but significant texture or geometric distortions are present, severely impacting the perception of the semantic meaning. 3: Semantic structure is largely correct and fully recognizable. Minor texture or structural distortions exist, but they do not lead to misinterpretation, and there are no major structural errors. 4: Generated texture and structure are natural, reasonable, and fully consistent with the input image.

A.4. Consistency of Human Evaluation

To ensure annotation consistency, we recruited professional annotators from the digital visual art industry, standardized the annotation workflow via a custom Gradio system with unified training, and implemented expert inspection to filter anomalies. To analyze inter-annotator agreement, a random 10% subset of

Model	Config ID	SmallFace Face	Crowd	Vehicles	Street View	Aerial View	Hands/ Feet	Complex Texture	Text	Digital Zoom	OP (Color)
HYPIR	1	2.83	2.00	3.00	2.71	2.90	2.68	2.58	2.50	2.17	2.23
	2	2.94	2.50	3.10	2.86	2.90	3.05	2.75	2.61	2.61	2.43
	3	2.61	2.10	3.20	2.71	2.70	2.73	2.58	2.50	2.26	2.14
PiSA-SR	1	1.78	1.60	2.30	2.00	1.80	2.64	2.17	2.22	2.15	1.67
	2	1.67	1.30	2.40	2.21	1.70	2.68	2.00	2.11	2.04	1.94
	3	1.28	1.10	2.00	1.79	1.40	2.41	2.08	2.06	1.96	1.44
SeeSR	1	2.28	1.70	2.20	2.21	1.70	2.30	2.17	1.78	2.20	2.30
	2	1.78	1.30	2.10	1.79	1.70	2.59	2.08	1.94	1.65	1.66
	3	1.72	1.40	2.00	1.71	1.70	2.41	1.92	1.94	1.57	1.54
DiffBIR	1	2.11	1.30	2.50	2.36	1.80	2.82	2.58	2.39	1.70	2.11
	2	2.06	1.40	2.70	2.29	2.40	2.59	2.17	2.17	1.98	2.26
	3	2.11	1.30	2.50	2.21	1.90	2.77	2.58	2.39	1.65	2.01
	4	2.06	1.40	2.80	2.50	2.30	2.50	2.17	2.22	2.07	2.26
SUPIR	1	2.44	1.40	2.80	2.71	2.50	2.68	2.08	2.17	1.85	1.77
	2	2.50	1.30	2.80	2.36	2.10	2.32	1.75	1.78	1.50	1.87
	3	2.50	1.70	2.70	2.64	2.70	2.86	2.33	2.33	1.87	1.44
	4	2.33	1.10	2.30	2.14	1.60	2.32	1.83	1.89	1.33	1.20

Table 7. Average overall scores of different parameter configurations across semantic categories. Bold numbers indicate the best-performing configuration within each model for a given category

the dataset was re-annotated. The Krippendorff’s Alpha coefficients [110] were 0.804/0.729/0.780/0.807 for Detail/Sharpness/Semantics/Overall dimensions. Statistically, these scores are well above the standard acceptance threshold of 0.667, demonstrating that our data reflects rigorous expert consensus rather than subjective noise.

B. Additional Results

B.1. More Score Distributions

We further provide score distributions for all remaining semantic categories that were not visualized in the main paper. Results for Overall Detail, Sharpness, and Semantics are shown in Figs. 12 and 19. We also report complete score distributions across all degradation types in Fig. 20.

B.2. More Results of Parameter Configurations

To support the parameter sensitivity study in the main paper, we evaluate multiple inference configurations for several diffusion-based GIR models. These configurations, as shown in Tab. 6 are chosen to intentionally vary the level of fidelity and generation, allowing us to obtain a richer and more diverse set of restoration outcomes. We further report the performance of each configuration across different semantic scenes and degradation types, as summarized in Tab. 7. Qualitative comparisons illustrating how different parameters affect restoration behavior can be found in Figs. 21 and 22. All configuration identifiers exactly match those reported in the main paper.

C. Qualitative Analysis of IQA

To complement the quantitative results in the main paper, we provide qualitative examples illustrating the limitations of existing IQA methods when evaluating generative image restoration. Although recent learning-based IQA models achieve strong performance on traditional distortions, they remain unreliable for GIR scenarios, particularly when semantic inconsistencies or generative artifacts are present.

In the Figs. 23 to 25, each case includes two restored outputs produced by different GIR models. For each restored image, we report the human-annotated overall scores, along with the predictions from several representative IQA models and our IQA model. These examples provide side-by-side comparisons of how IQA models and human annotators evaluate the same pair of restored images, allowing to directly observe the differences in their judgments.

D. More Failure Cases

To further support the observations discussed in the main paper, we present additional failure cases of current GIR models across a wide range of semantic scenes and degradation types. These examples cover various representative failure modes, including semantic errors in Figs. 26 and 27, over-generation of details in Fig. 28, and insufficient degradation removal in Fig. 29, providing a more complete visual reference of the behaviors discussed in the main paper.

E. Detail Results of each model

In the main paper, we primarily analyzed restoration behaviors at the model-family level. Here, we provide model-

Model	Average Overall Score \uparrow	Average Rank \downarrow
HYPIR	2.775	3.127
PiSA-SR	2.508	5.547
TSD-SR	2.467	7.487
DiffBIR	2.428	5.181
PASD	2.38	6.382
OSDiff	2.377	6.173
Invsr	2.279	7.635
SUPIR	2.235	9.062
SeeSR	2.201	8.870
CCSR	2.195	10.365
S3Diff	2.181	8.484
FLUX	1.935	12.099
StableSR	1.925	11.133
SwinIR	1.625	15.569
RealESRGAN	1.548	15.734
ResShift	1.466	13.858
BSRGAN	1.435	15.037
HAT	1.426	16.159
Nano Banana	1.401	15.552
CAL-GAN	1.246	16.544

Table 8. Overall performance ranking of all evaluated restoration models. We report each model’s mean overall quality score across the full dataset and its average per-image ranking position.

specific results, reporting the detailed performance of all 20 restoration models across all evaluation dimensions.

We first present the overall performance ranking of each model in Tab. 8, computed in two complementary ways: (1) the average overall quality score across the entire dataset, and (2) the average per-image ranking position, which reflects how frequently a model outperforms others on individual samples.

We then report per-degradation and per-semantic results for every evaluation dimension in Tabs. 10 to 16. Note that the Detail and Sharpness scores are calculated by taking the absolute value first, and then averaging the scores. And since 0 is the point of balance, a lower score indicates a better performance for these two dimensions. This includes the mean score of each model under every degradation type and semantic category, allowing comparison between different models.

F. More Details of our IQA Model

F.1. Training Details

To evaluate the restored images across four distinct dimensions, we train a dedicated model for each specific direction. Notably, the original **Detail** and **Sharpness** assessments are bipolar metrics, with subjective scores ranging from -3 to 3 , where 0 represents the optimal perceptual quality. To facilitate effective learning, we introduce a data preprocessing step that decouples these bipolar metrics into unipolar ones. For the **Detail** dimension, we utilize the data subset with **Detail** scores ≥ 0 to train a model for predicting **Con-**

Test set	NIQE	MANIQA	MUSIQ	CLIP-IQA	DeQA-Score	Ours
LIVEW	0.81/0.77	0.85/0.83	0.79/0.83	<u>0.83/0.81</u>	0.89/0.88	<u>0.83/0.81</u>
AGIQA	0.72/0.65	0.72/0.64	0.72/0.63	0.74/0.69	0.81/0.73	0.81/0.76
CSIQ	0.70/0.65	0.62/0.63	0.77/0.71	0.77/0.72	<u>0.79/0.74</u>	0.86/0.83

Table 9. Performance comparison of our proposed method against popular IQA models on three external datasets. Results are reported in terms of SRCC/PLCC. The best and second-best results are highlighted in **bold** and underlined respectively.

tent Conciseness, while the subset with scores ≤ 0 is used to train the model for assessing **Detail Completeness**. For the **Sharpness** dimension, we utilize the data subset with **Sharpness** scores ≥ 0 to train a model for predicting **Visual Clarity**, while the subset with scores ≤ 0 is used to train the model for assessing **Visual Clarity**. The overall training protocol and hyperparameter configurations for our IQA models strictly follow those established in DeQA[73].

F.2. Generalization

We evaluated our model on three distinct external datasets; the results (SRCC/PLCC) are as shown in Tab. 9. While other models predict only overall quality, we provide a multi-dimensional IQA model that independently assesses Detail, Sharpness, and Semantics, enabling fine-grained evaluation.



Large Face



Medium Face



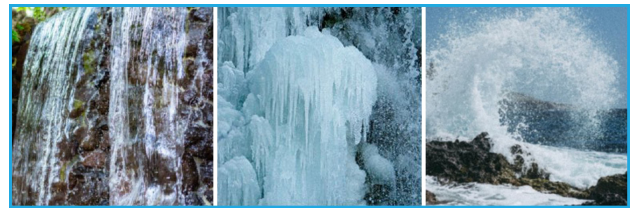
Small Face



Crowd



Animal Fur



Water Flow



Reflective Glass



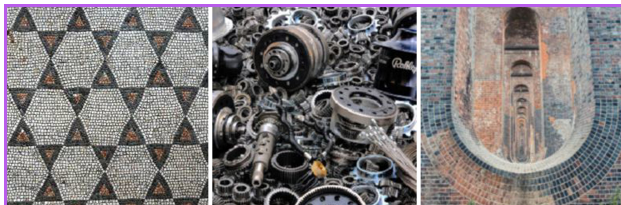
Trees & leaves



Fabric Texture



Leather Surface



Complex texture



Vehicles



Street View



Architecture

Figure 13. More low-quality examples of different semantic categories. Zoom in for a better view.



Food



Aerial View



Hands/Feet



Text



Print Media



Cartoon/Comic



Hand-drawn

Figure 14. More low-quality examples of different semantic categories. Zoom in for a better view.



Old Photo (Color)



Old Film

Figure 15. More visual examples of different degradation categories. Zoom in for a better view.



Surveillance



Digital Zoom



Low Light



Compression



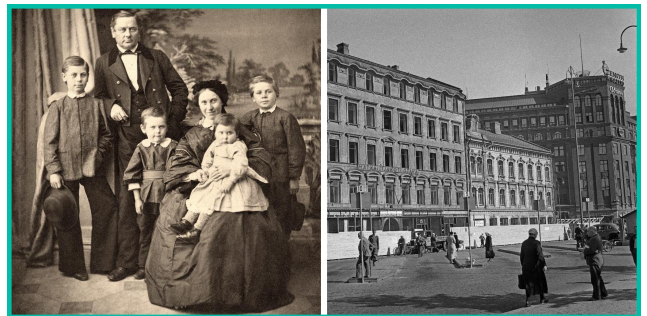
Motion Blur



Defocus Blur



ISP Noise



Old Photo (B/W)

Figure 16. More visual examples of different degradation categories. Zoom in for a better view.

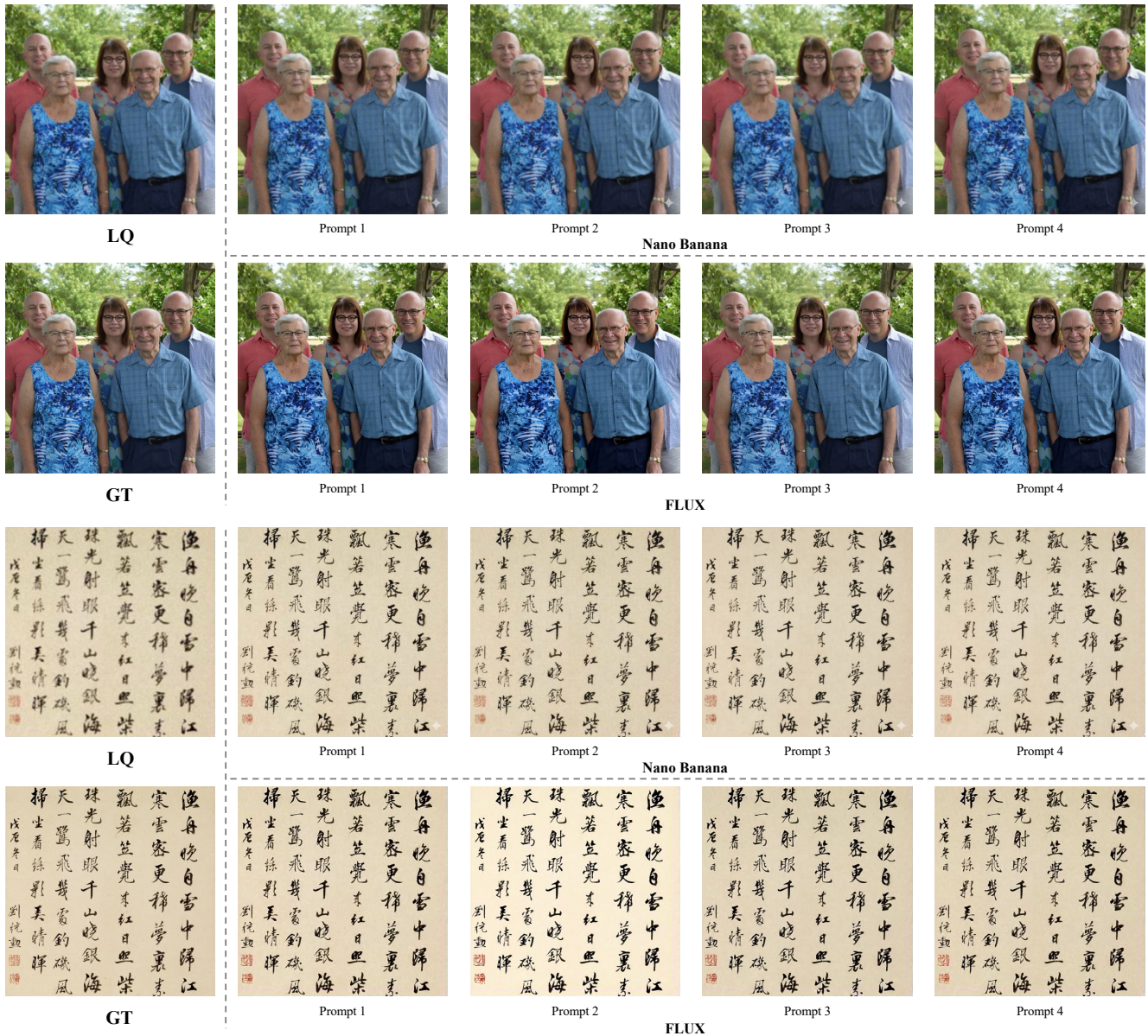


Figure 17. Results of different prompts used in generation models. Zoom in for a better view.

Prompt 1: Perform high-quality image restoration and super-resolution in this image: enhance clarity, remove noise and scratches, reduce blur, and sharpen fine details|while preserving a natural, realistic appearance without over-processing or artificial artifacts.

Prompt 2: Restore this image with enhanced clarity and sharpness. Reduce noise, fix compression artifacts, and improve detail while strictly preserving the original content, style, and semantics.

Prompt 3: Clean and restore the image by removing artifacts, noise, and blur. Maintain full fidelity to the original composition and avoid creating new visual elements.

Prompt 4: Improve this image's perceptual quality: refine edges, correct degradation, and enhance fine details. Do not alter identity, expression, or any semantic attributes.

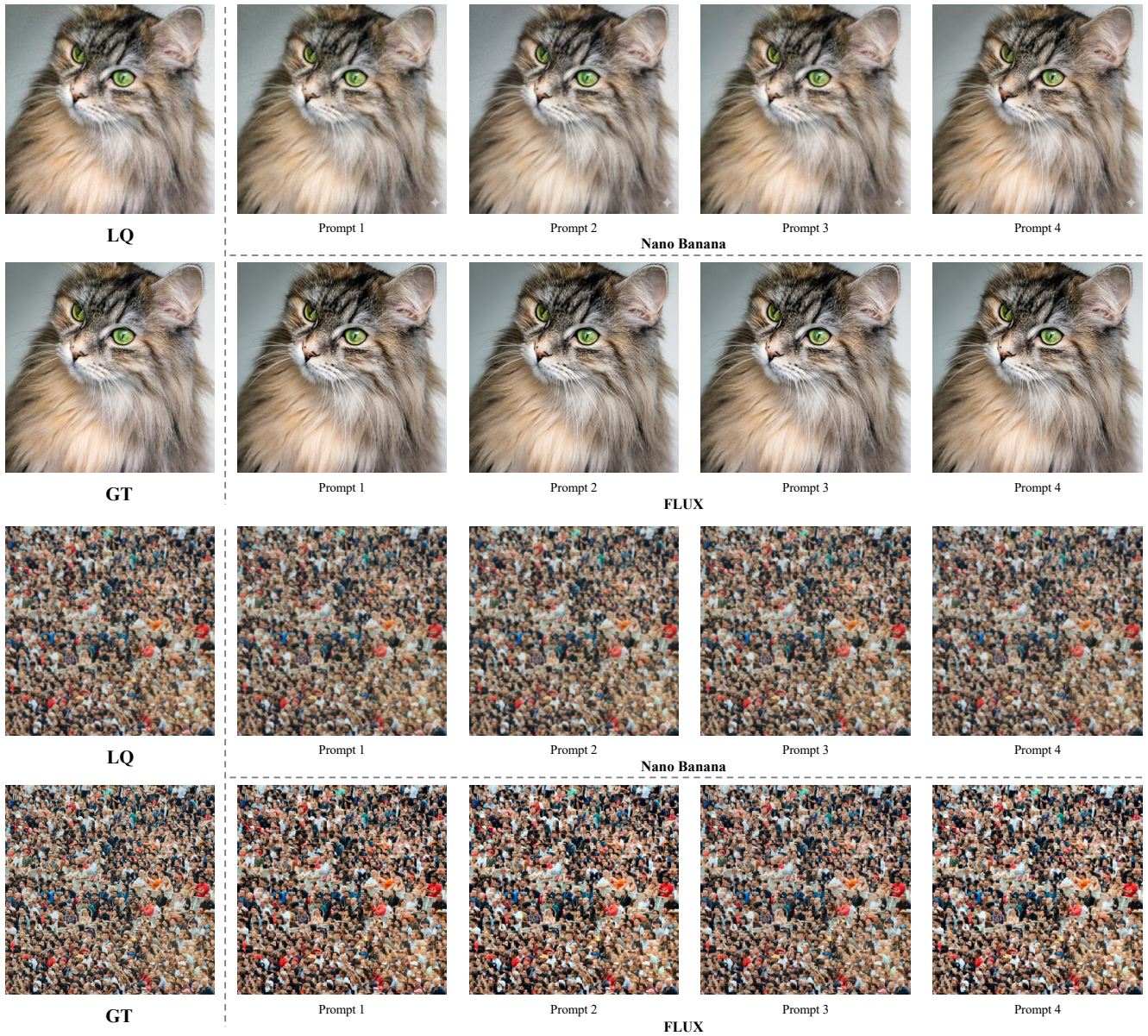


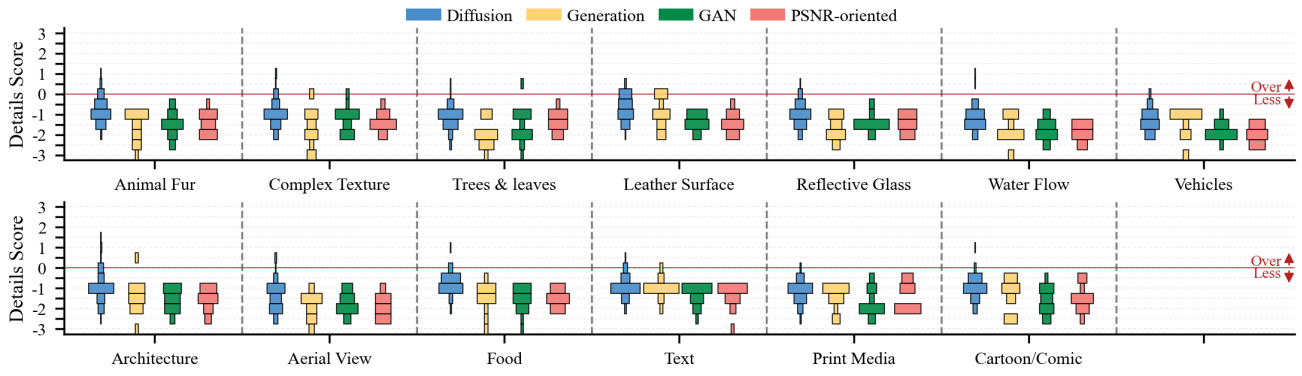
Figure 18. Results of different prompts used in generation models. Zoom in for a better view.

Prompt 1: Perform high-quality image restoration and super-resolution in this image: enhance clarity, remove noise and scratches, reduce blur, and sharpen fine details|while preserving a natural, realistic appearance without over-processing or artificial artifacts.

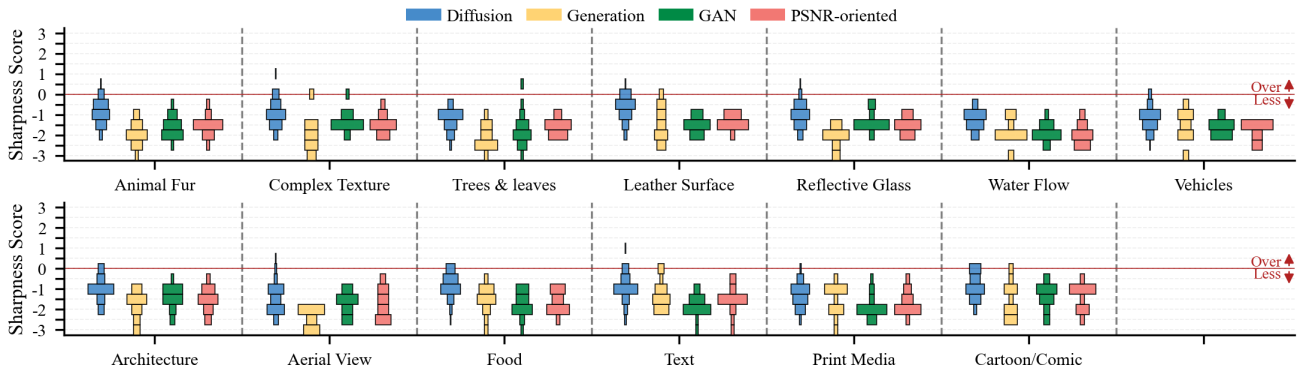
Prompt 2: Restore this image with enhanced clarity and sharpness. Reduce noise, fix compression artifacts, and improve detail while strictly preserving the original content, style, and semantics.

Prompt 3: Clean and restore the image by removing artifacts, noise, and blur. Maintain full fidelity to the original composition and avoid creating new visual elements.

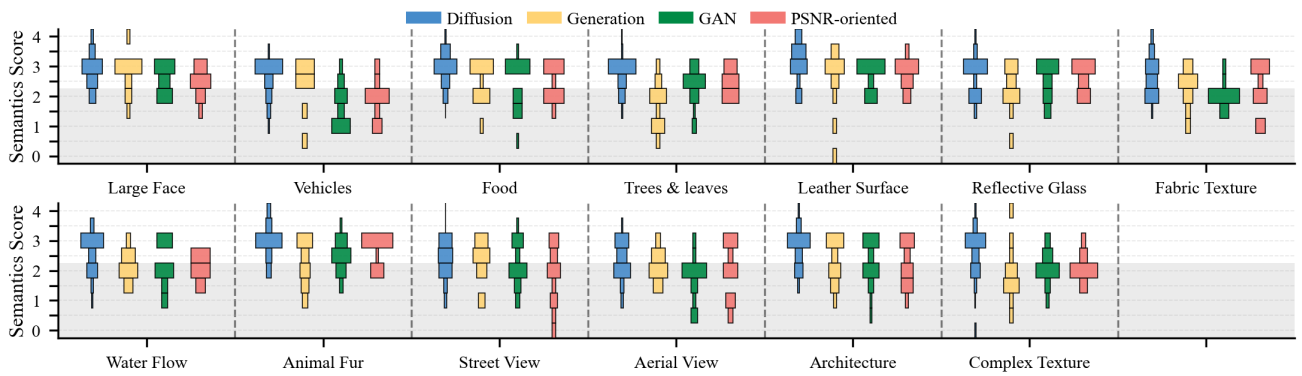
Prompt 4: Improve this image's perceptual quality: refine edges, correct degradation, and enhance fine details. Do not alter identity, expression, or any semantic attributes.



(a) Distribution of detail scores across semantic scene groups.

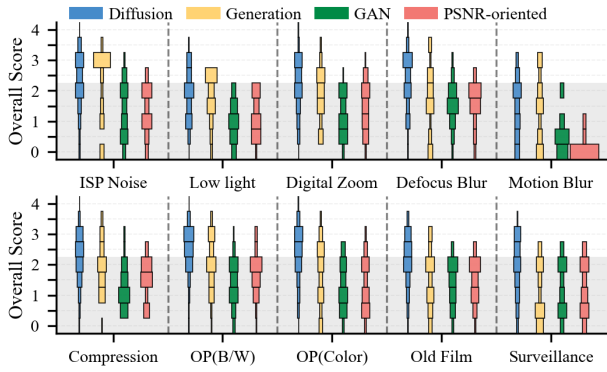


(b) Distribution of sharpness scores across semantic scene groups.

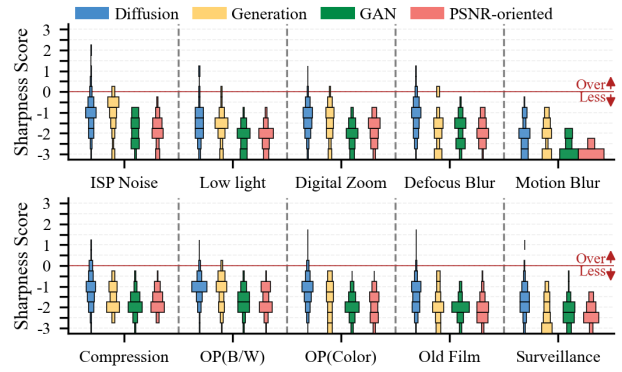


(c) Distribution of semantic scores across semantic scene groups.

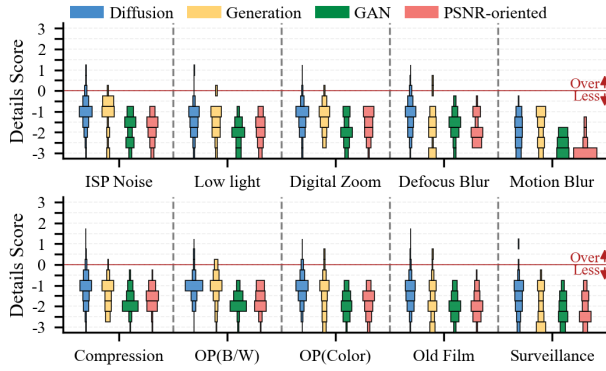
Figure 19. Distribution of different scores across various semantic scene groups. The horizontal width of each box indicates the percentage of samples within each score interval. The red line indicates the balance point; scores above it (*Over* ↑) denote over-generation, and scores below it (*Less* ↓) denote under-generation. The light gray region indicates low overall scores, representing generally unacceptable results.



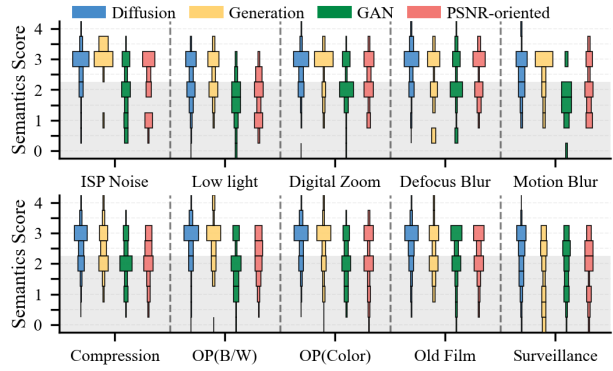
(a) Distribution of overall scores across degradations.



(b) Distribution of semantic scores across degradations.



(c) Distribution of detail scores across degradations.



(d) Distribution of sharpness scores across degradations.

Figure 20. Distribution of different scores across various degradation types. The horizontal width of each box indicates the percentage of samples within each score interval. The light gray region indicates low overall scores, representing generally unacceptable results. The red line indicates the balance point; scores above it (**Over** ↑) denote over-generation, and scores below it (**Less** ↓) denote under-generation.

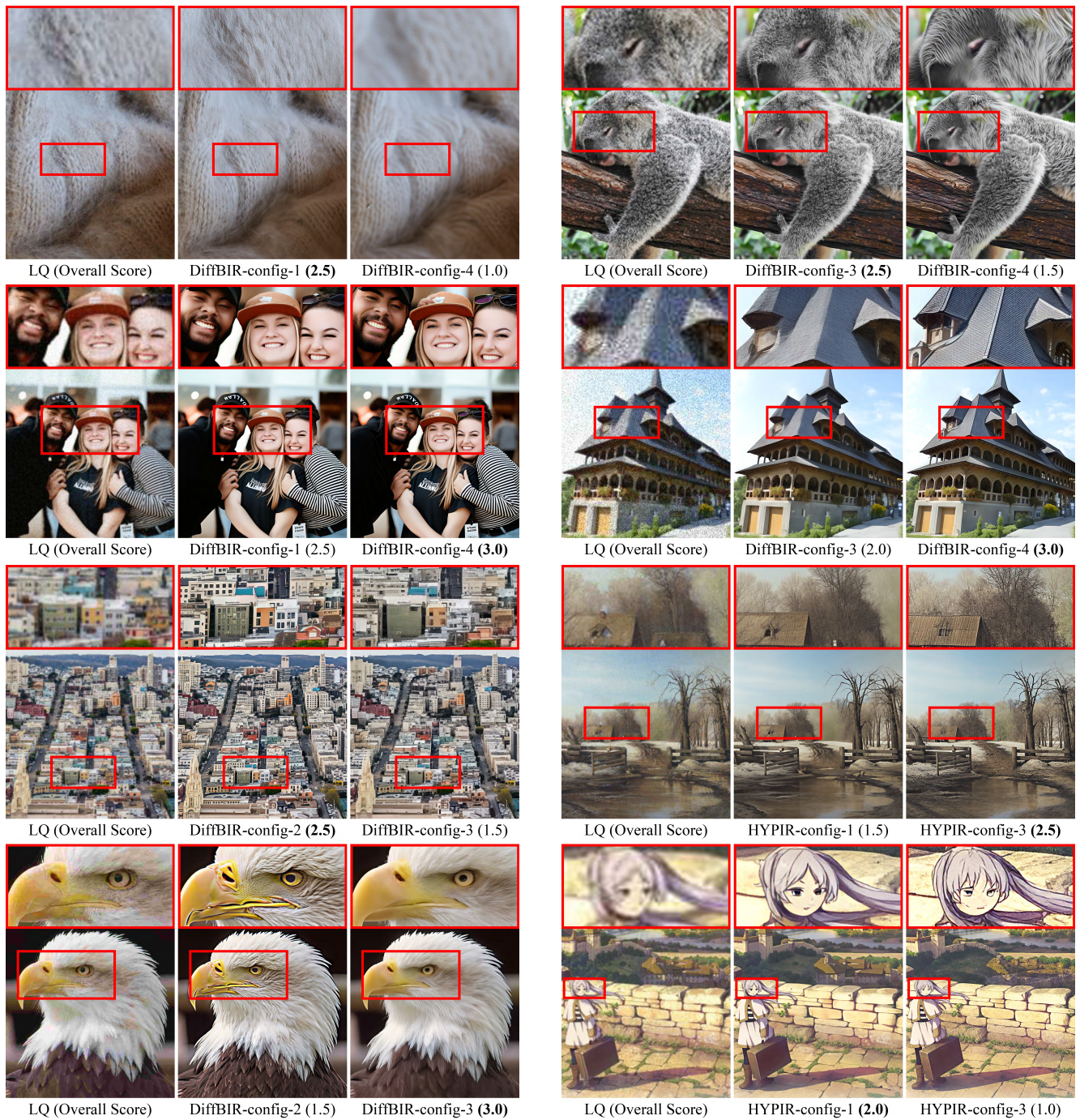


Figure 21. Effect of parameter configurations on restoration behavior in diffusion-based models. Zoom in for a better view.

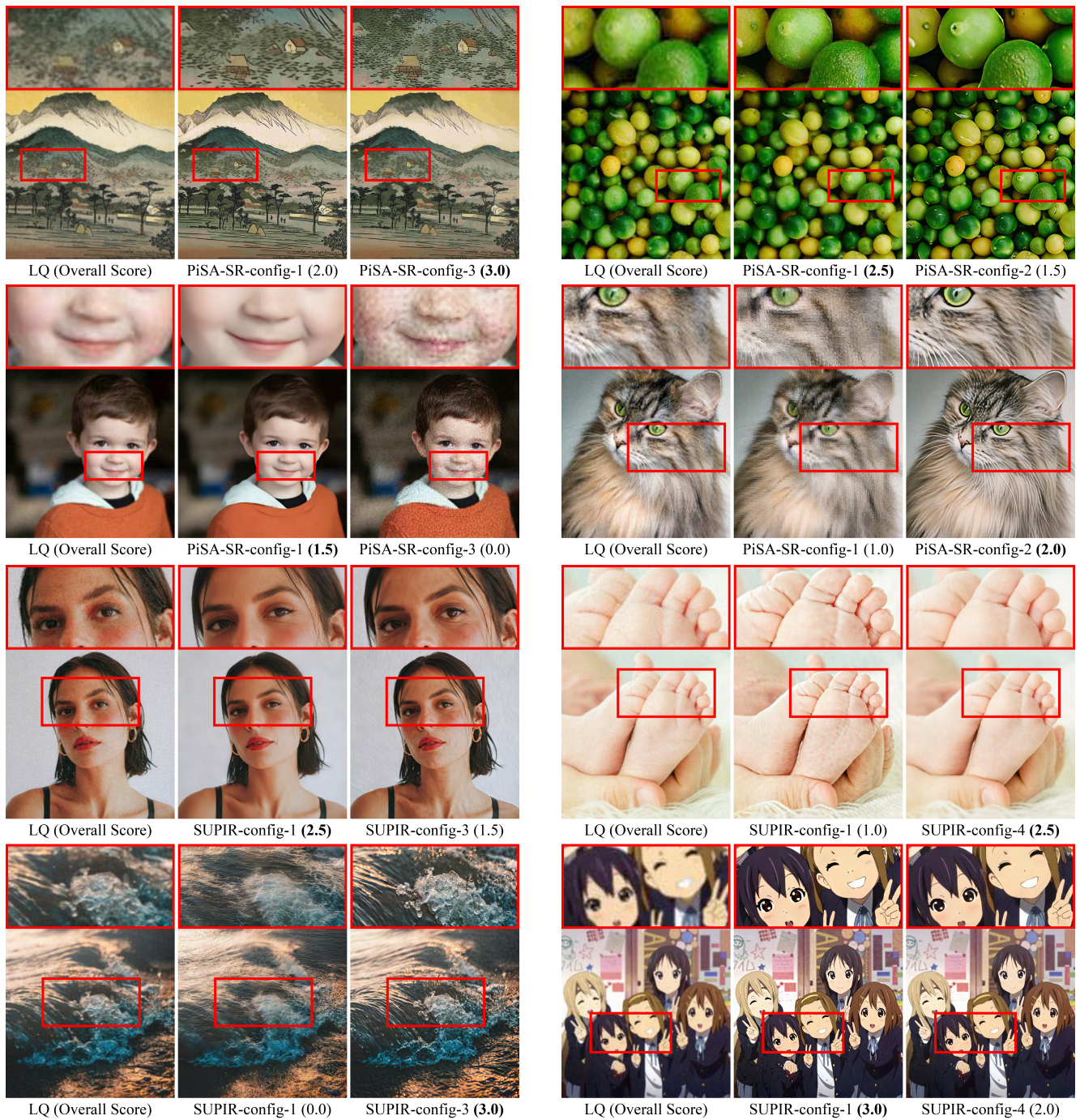


Figure 22. Effect of parameter configurations on restoration behavior in diffusion-based models. Zoom in for a better view.



Image A

Image B

	NIQE↓	PI↓	MANIQA	CLIP-IQA	MUSIQ	DeQA-Score	Ours	Human
Image A	3.61	3.46	0.214	0.527	69.7	4.11	4.29	3.5
Image B	2.78	2.93	0.262	0.635	71.3	4.27	3.62	2
Better	B	B	B	B	B	B	A	A

$E_{z \sim p_{adv}} [\log D_G^c(x)] + E_{z \sim p_s} [\log (1 - D_G^c(G(z)))]$

$E_{z \sim p_{adv}} [\log D_G^c(x)] + E_{z \sim p_s} [\log (1 - D_G^c(G(z)))]$

$E_{z \sim p_{adv}} [\log \frac{p_{adv}(z)}{\|p_{adv}(z) + p_s(z)\|}]$

$D_G^c(x) = \frac{p_{adv}(x)}{p_{adv}(x) + p_s(x)}$

The minmax game in (1) can be reformulated:

$C(G) = \max_V V(D, G)$

$= \max_{z \sim p_{adv}} [\log D_G^c(x)] + E_{z \sim p_s} [\log (1 - D_G^c(G(z)))]$

$= \max_{z \sim p_{adv}} [\log \frac{p_{adv}(z)}{\|p_{adv}(z) + p_s(z)\|}] + E_{z \sim p_s} [\log \frac{p_s(z)}{\|p_{adv}(z) + p_s(z)\|}] - 2 \log 2$

The definition of Kullback-Leibler (KL) divergence between two distributions $p(x)$ and $q(x)$ are defined as:

$KL(p||q) = \int p(x) \log \frac{p(x)}{q(x)} dx$

$JS(p||q) = \frac{1}{2} KL(p||\frac{p+q}{2}) + \frac{1}{2} KL(q||\frac{p+q}{2})$

Therefore, (3) is equal to:

$C(G) = KL(p_{adv}||\frac{p_{adv}+p_s}{2}) + KL(p_s||\frac{p_{adv}+p_s}{2}) - 2 \log 2$

$= 2 JS(p_{adv}||p_s) - 2 \log 2$

Thus, the objective function of GANs is related to JS-divergence and JS-divergence.

the original GANs. Then,

$E_{z \sim p_{adv}} [\log D_G^c(x)] + E_{z \sim p_s} [\log (1 - D_G^c(G(z)))]$

$E_{z \sim p_{adv}} [\log D_G^c(x)] + E_{z \sim p_s} [\log (1 - D_G^c(G(z)))]$

$E_{z \sim p_{adv}} [\log \frac{p_{adv}(z)}{\|p_{adv}(z) + p_s(z)\|}]$

$D_G^c(x) = \frac{p_{adv}(x)}{p_{adv}(x) + p_s(x)}$

The minmax game in (1) can be reformulated:

$C(G) = \max_V V(D, G)$

$= \max_{z \sim p_{adv}} [\log D_G^c(x)] + E_{z \sim p_s} [\log (1 - D_G^c(G(z)))]$

$= \max_{z \sim p_{adv}} [\log \frac{p_{adv}(z)}{\|p_{adv}(z) + p_s(z)\|}] + E_{z \sim p_s} [\log \frac{p_s(z)}{\|p_{adv}(z) + p_s(z)\|}] - 2 \log 2$

The definition of Kullback-Leibler (KL) divergence between two distributions $p(x)$ and $q(x)$ are defined as:

$KL(p||q) = \int p(x) \log \frac{p(x)}{q(x)} dx$

$JS(p||q) = \frac{1}{2} KL(p||\frac{p+q}{2}) + \frac{1}{2} KL(q||\frac{p+q}{2})$

Therefore, (3) is equal to:

$C(G) = KL(p_{adv}||\frac{p_{adv}+p_s}{2}) + KL(p_s||\frac{p_{adv}+p_s}{2}) - 2 \log 2$

$= 2 JS(p_{adv}||p_s) - 2 \log 2$

Thus, the objective function of GANs is related to JS-divergence and JS-divergence.

the original GANs. Then,

Image A

Image B

	NIQE↓	PI↓	MANIQA	CLIP-IQA	MUSIQ	DeQA-Score	Ours	Human
Image A	13.2	8.70	0.290	0.644	58.8	3.70	3.63	3.5
Image B	9.09	6.56	0.338	0.606	60.4	3.56	3.41	2
Better	B	B	B	B	B	A	A	A



Image A

Image B

	NIQE↓	PI↓	MANIQA	CLIP-IQA	MUSIQ	DeQA-Score	Ours	Human
Image A	3.38	3.45	0.161	0.463	67.2	4.00	3.01	2.5
Image B	3.20	3.20	0.250	0.621	71.8	4.00	2.29	1.5
Better	B	B	B	B	B	-	A	A

$E_{z \sim p_{adv}} [\log D_G^c(x)] + E_{z \sim p_s} [\log (1 - D_G^c(G(z)))]$

$E_{z \sim p_{adv}} [\log D_G^c(x)] + E_{z \sim p_s} [\log (1 - D_G^c(G(z)))]$

$E_{z \sim p_{adv}} [\log \frac{p_{adv}(z)}{\|p_{adv}(z) + p_s(z)\|}]$

$D_G^c(x) = \frac{p_{adv}(x)}{p_{adv}(x) + p_s(x)}$

The minmax game in (1) can be reformulated:

$C(G) = \max_V V(D, G)$

$= \max_{z \sim p_{adv}} [\log D_G^c(x)] + E_{z \sim p_s} [\log (1 - D_G^c(G(z)))]$

$= \max_{z \sim p_{adv}} [\log \frac{p_{adv}(z)}{\|p_{adv}(z) + p_s(z)\|}] + E_{z \sim p_s} [\log \frac{p_s(z)}{\|p_{adv}(z) + p_s(z)\|}] - 2 \log 2$

The definition of Kullback-Leibler (KL) divergence between two distributions $p(x)$ and $q(x)$ are defined as:

$KL(p||q) = \int p(x) \log \frac{p(x)}{q(x)} dx$

$JS(p||q) = \frac{1}{2} KL(p||\frac{p+q}{2}) + \frac{1}{2} KL(q||\frac{p+q}{2})$

Therefore, (3) is equal to:

$C(G) = KL(p_{adv}||\frac{p_{adv}+p_s}{2}) + KL(p_s||\frac{p_{adv}+p_s}{2}) - 2 \log 2$

$= 2 JS(p_{adv}||p_s) - 2 \log 2$

Thus, the objective function of GANs is related to JS-divergence and JS-divergence.

the original GANs. Then,

$E_{z \sim p_{adv}} [\log D_G^c(x)] + E_{z \sim p_s} [\log (1 - D_G^c(G(z)))]$

$E_{z \sim p_{adv}} [\log D_G^c(x)] + E_{z \sim p_s} [\log (1 - D_G^c(G(z)))]$

$E_{z \sim p_{adv}} [\log \frac{p_{adv}(z)}{\|p_{adv}(z) + p_s(z)\|}]$

$D_G^c(x) = \frac{p_{adv}(x)}{p_{adv}(x) + p_s(x)}$

The minmax game in (1) can be reformulated:

$C(G) = \max_V V(D, G)$

$= \max_{z \sim p_{adv}} [\log D_G^c(x)] + E_{z \sim p_s} [\log (1 - D_G^c(G(z)))]$

$= \max_{z \sim p_{adv}} [\log \frac{p_{adv}(z)}{\|p_{adv}(z) + p_s(z)\|}] + E_{z \sim p_s} [\log \frac{p_s(z)}{\|p_{adv}(z) + p_s(z)\|}] - 2 \log 2$

The definition of Kullback-Leibler (KL) divergence between two distributions $p(x)$ and $q(x)$ are defined as:

$KL(p||q) = \int p(x) \log \frac{p(x)}{q(x)} dx$

$JS(p||q) = \frac{1}{2} KL(p||\frac{p+q}{2}) + \frac{1}{2} KL(q||\frac{p+q}{2})$

Therefore, (3) is equal to:

$C(G) = KL(p_{adv}||\frac{p_{adv}+p_s}{2}) + KL(p_s||\frac{p_{adv}+p_s}{2}) - 2 \log 2$

$= 2 JS(p_{adv}||p_s) - 2 \log 2$

Thus, the objective function of GANs is related to JS-divergence and JS-divergence.

the original GANs. Then,

Image A

Image B

	NIQE↓	PI↓	MANIQA	CLIP-IQA	MUSIQ	DeQA-Score	Ours	Human
Image A	3.72	3.73	0.184	0.513	64.6	3.32	3.33	2.5
Image B	3.68	3.37	0.206	0.676	63.4	3.39	2.25	2
Better	B	B	B	B	A	B	A	A

Figure 23. Qualitative analysis of image quality assessment methods. Zoom in for a better view.

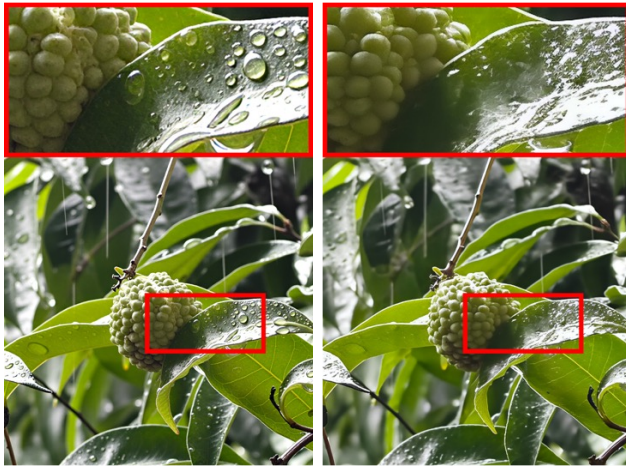


Image A

Image B

	NIQE↓	PI↓	MANIQA	CLIP-IQA	MUSIQ	DeQA-Score	Ours	Human
Image A	3.98	3.80	0.244	0.826	74.6	4.51	4.01	3
Image B	3.99	3.73	0.254	0.837	76.3	4.55	3.68	1.5
Better	A	B	B	B	B	B	A	A

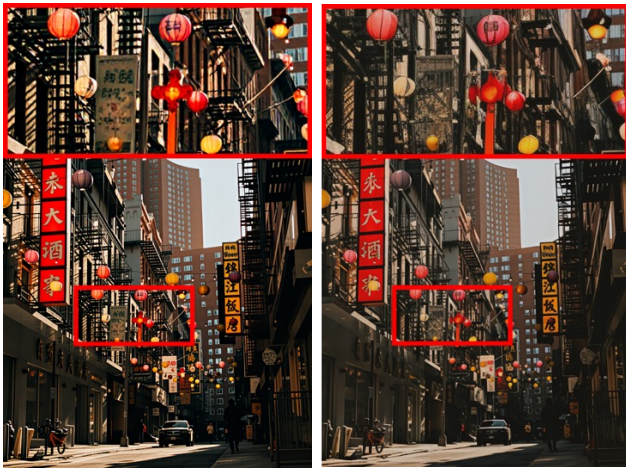


Image A

Image B

	NIQE↓	PI↓	MANIQA	CLIP-IQA	MUSIQ	DeQA-Score	Ours	Human
Image A	4.36	3.95	0.266	0.453	70.3	3.98	3.69	3
Image B	3.11	3.08	0.272	0.524	70.9	4.00	3.28	2
Better	B	B	B	B	B	B	A	A

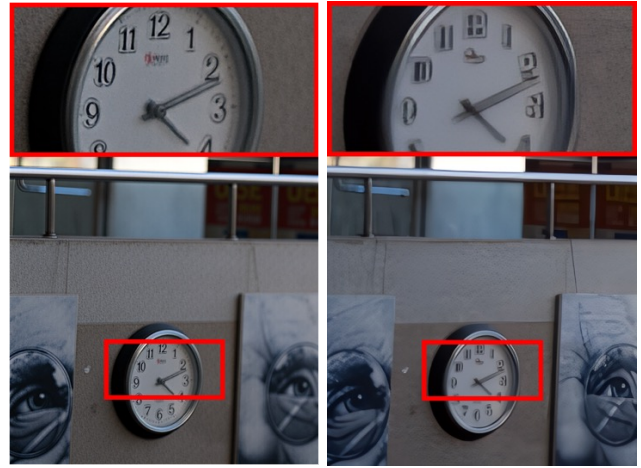


Image A

Image B

	NIQE↓	PI↓	MANIQA	CLIP-IQA	MUSIQ	DeQA-Score	Ours	Human
Image A	4.76	3.71	0.149	0.442	52.0	3.68	3.92	3
Image B	4.52	4.09	0.163	0.486	57.7	3.91	3.12	1.5
Rank	B	A	B	B	B	B	A	A



Image A

Image B

	NIQE↓	PI↓	MANIQA	CLIP-IQA	MUSIQ	DeQA-Score	Ours	Human
Image A	3.37	3.30	0.298	0.461	74.2	4.40	3.10	2.5
Image B	2.27	2.71	0.277	0.637	76.3	4.48	2.94	2
Better	B	B	A	B	B	B	A	A

Figure 24. Qualitative analysis of image quality assessment methods. Zoom in for a better view.



Image A

Image B

	NIQE↓	PI↓	MANIQA	CLIP-IQA	MUSIQ	DeQA-Score	Ours	Human
Image A	4.25	3.85	0.169	0.589	62.3	3.70	3.14	2.5
Image B	3.76	3.46	0.215	0.801	71.3	4.03	3.07	2
Better	B	B	B	B	B	B	A	A



Image A

Image B

	NIQE↓	PI↓	MANIQA	CLIP-IQA	MUSIQ	DeQA-Score	Ours	Human
Image A	4.53	3.74	0.204	0.762	68.9	3.37	3.41	3.5
Image B	3.11	3.04	0.346	0.833	73.3	3.53	3.27	2
Better	B	B	B	B	B	B	A	A

Figure 25. Qualitative analysis of image quality assessment methods. Zoom in for a better view.

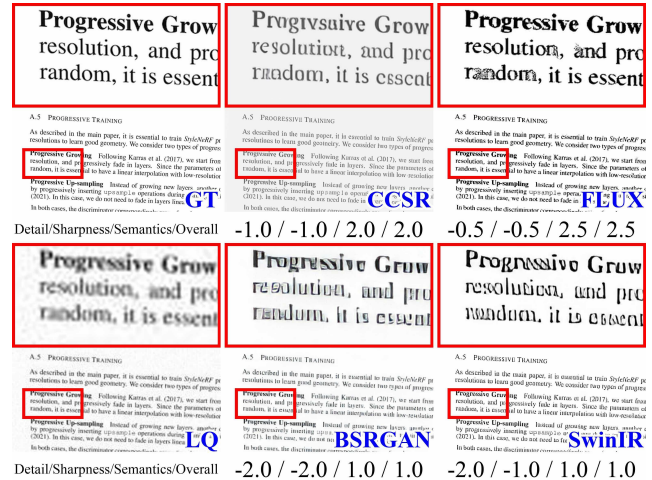
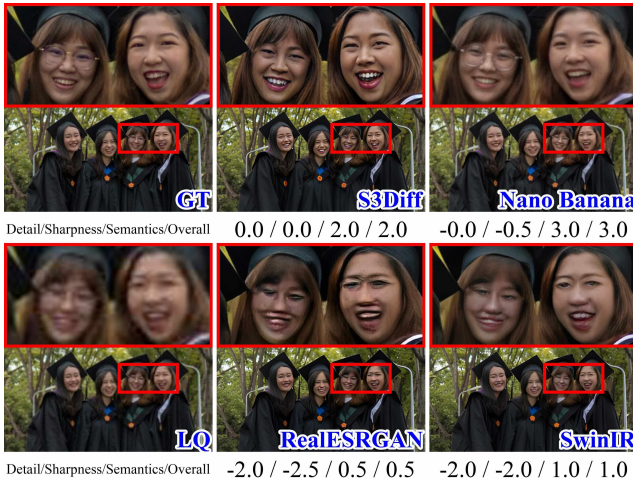


Figure 26. Failure cases of semantic errors. Zoom in for a better view.



Figure 27. Failure cases of semantic errors. Zoom in for a better view.

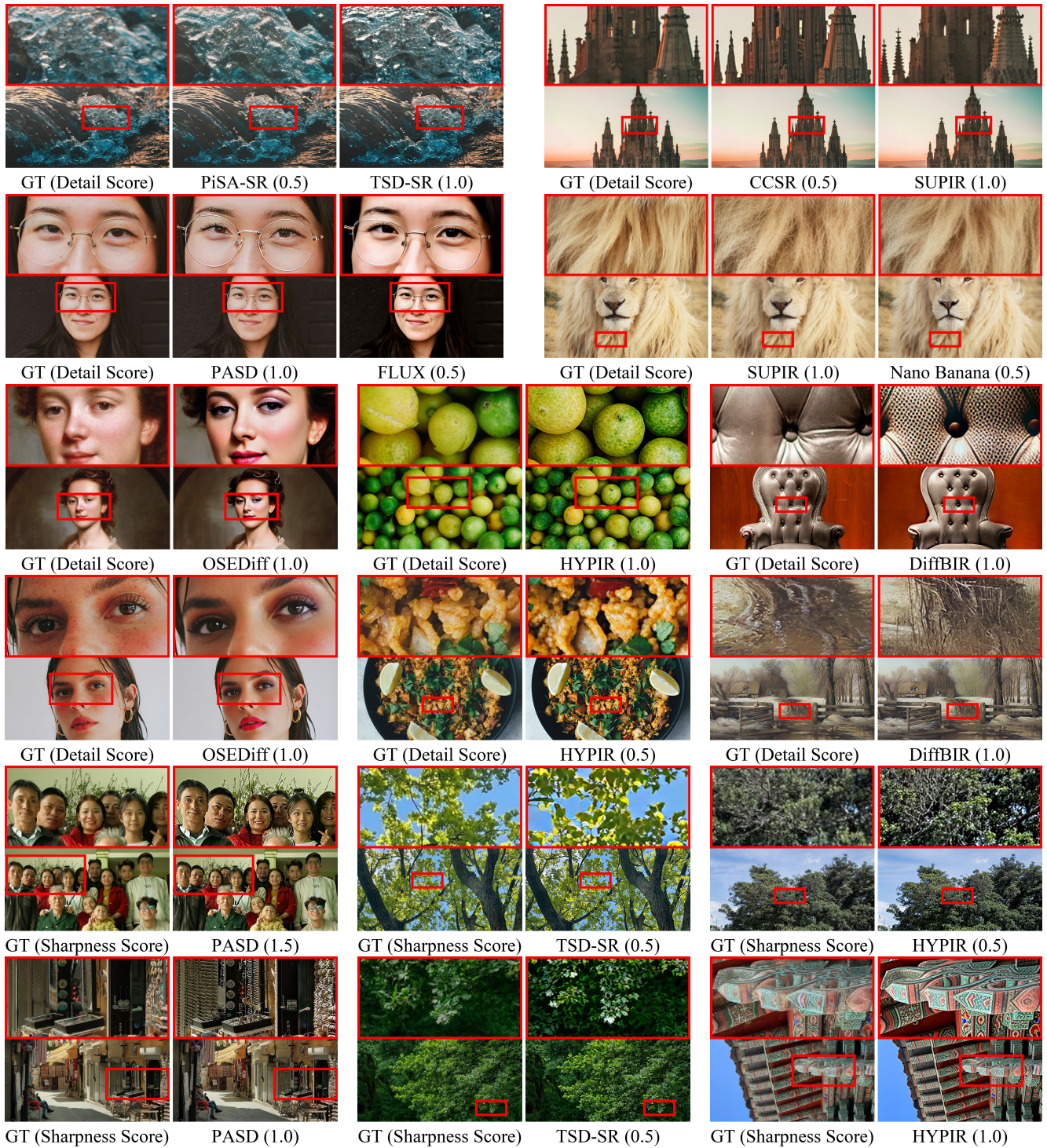


Figure 28. Failure cases of over-generation. Zoom in for a better view.

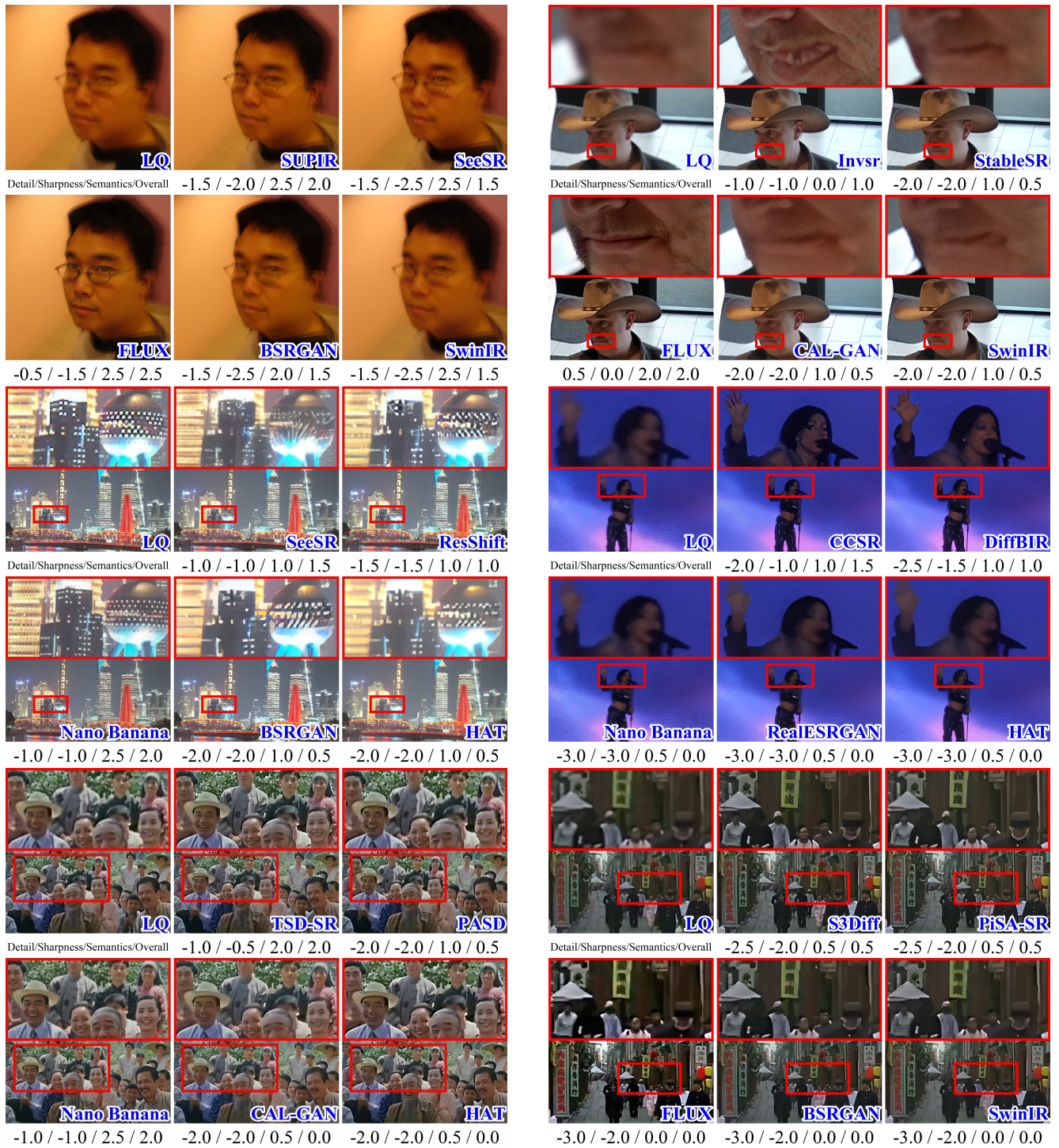


Figure 29. Failure cases of hard degradations. Zoom in for a better view.

Model	Large Face			Medium Face			Small Face			
	Overall↑	Sharpness↓	Detail↓	Overall↑	Sharpness↓	Detail↓	Overall↑	Sharpness↓	Detail↓	
HYPIR	3.07	0.57	0.57	3.14	0.94	0.78	3.17	1.17	1.00	2.89
SUPIR	2.57	1.14	0.93	2.79	1.39	1.06	2.72	1.56	1.06	2.56
PISA-SR	2.64	1.07	1.36	2.86	1.22	1.06	2.94	1.44	1.44	2.67
SeeSR	2.57	1.43	1.36	2.71	2.39	1.44	2.72	1.39	1.39	2.22
OSDiff	2.64	1.36	1.43	3.21	2.44	1.44	2.50	1.61	1.67	2.28
CCSR	2.57	0.29	1.00	2.93	2.56	0.94	2.72	1.28	1.50	2.17
DiffBIR	3.00	0.79	0.93	3.14	2.78	1.17	2.94	1.22	1.50	2.44
StablesR	2.21	1.64	1.50	2.79	2.06	1.61	2.44	2.06	1.83	2.22
PASD	2.71	0.79	0.86	2.93	2.22	1.11	2.44	0.72	0.67	2.11
Invsr	2.43	1.07	1.07	2.79	2.44	1.17	2.61	1.28	1.50	2.39
S3Diff	3.00	0.93	0.79	3.07	2.78	0.72	2.89	1.06	1.22	2.44
TSD-SR	2.50	1.07	1.07	2.71	2.56	1.06	2.72	1.33	1.28	2.50
ResShift	1.86	2.07	1.79	2.14	1.61	1.89	2.22	1.83	1.83	1.72
FLUX	2.14	1.21	1.14	2.71	2.44	1.00	2.78	1.44	1.44	2.39
Nano Banana	1.71	1.71	1.57	2.79	1.89	1.39	2.50	2.44	2.28	2.11
BSRGAN	2.00	2.00	1.71	2.71	1.83	2.06	2.39	2.17	2.11	1.39
CAL-GAN	1.79	2.00	1.71	2.50	1.50	1.94	2.06	2.17	2.08	1.67
RealESRGAN	1.71	2.14	2.00	2.43	1.83	1.83	2.39	1.94	2.17	1.56
HAT	1.71	2.21	1.93	2.36	1.56	2.06	2.06	2.39	2.39	1.44
SwinIR	2.07	1.71	1.64	2.57	1.83	1.83	2.28	1.78	2.17	1.67

Table 10. The result of average overall, sharpness, detail, and semantics scores for all restoration models in Large Face, Large Face and Small Face. Note that the Detail and Sharpness scores are calculated by taking the absolute value first, and then averaging the scores.

Model	Crowd			Hands/Feet			Animal Fur				
	Overall↑	Sharpness↓	Detail↓	Overall↑	Sharpness↓	Detail↓	Overall↑	Sharpness↓	Detail↓		
HYPIR	2.40	1.30	1.50	2.40	3.05	0.80	3.15	2.94	0.50	0.67	3.11
SUPIR	1.80	1.70	1.80	1.70	2.55	1.25	2.75	2.89	1.00	0.78	3.11
PISA-SR	1.90	1.60	1.60	1.70	2.40	1.15	2.60	3.06	0.72	0.56	3.22
SeeSR	1.70	1.60	1.80	1.40	2.30	1.40	2.45	2.50	1.17	1.17	2.83
OSDiff	1.20	1.80	1.90	1.50	2.40	1.15	2.50	2.72	1.06	0.83	3.06
CCSR	0.90	1.80	2.00	1.40	2.25	1.30	2.35	2.83	0.72	0.61	3.00
DiffBIR	1.60	1.70	1.70	1.60	2.40	0.80	2.60	3.06	0.50	0.72	3.11
StablesR	1.30	1.80	1.90	1.20	1.70	1.75	2.20	2.28	1.67	1.39	2.61
PASD	1.70	1.40	1.50	1.90	2.25	1.10	2.50	2.78	0.89	0.94	2.94
Invsr	1.80	1.80	1.70	1.60	2.40	1.10	2.60	3.00	0.56	0.72	3.00
S3Diff	2.00	1.40	1.60	1.80	2.80	0.95	2.90	3.17	0.67	0.67	3.22
TSD-SR	1.80	1.70	1.80	1.40	2.30	1.25	2.25	2.67	0.89	0.83	2.78
ResShift	1.10	1.80	2.00	1.30	1.55	1.75	2.00	2.11	1.44	1.28	2.61
FLUX	1.40	1.60	1.60	1.50	1.95	1.45	2.30	1.67	1.94	1.67	2.22
Nano Banana	0.20	2.70	2.50	1.30	1.05	2.40	1.90	1.78	1.94	1.56	2.22
BSRGAN	1.00	2.00	2.00	0.90	1.45	1.60	1.95	1.78	1.67	1.72	2.44
CAL-GAN	0.80	2.20	2.10	1.20	1.35	1.80	1.90	1.83	1.67	1.28	2.44
RealESRGAN	1.30	2.00	2.20	1.40	1.40	1.70	1.85	2.11	1.50	1.50	2.56
HAT	0.80	2.10	2.20	0.90	1.60	1.85	1.80	2.28	1.72	1.50	2.72
SwinIR	0.90	1.40	1.80	1.00	1.50	2.00	2.05	2.28	1.39	1.39	2.67

Table 11. The result of average overall, sharpness, detail, and semantics scores for all restoration models in Crowd, Crowd and Animal Fur. Note that the Detail and Sharpness scores are calculated by taking the absolute value first, and then averaging the scores.

Model	Complex Texture			Trees & leaves			Fabric Texture		
	Overall↑	Sharpness↓	Detail↓	Overall↑	Sharpness↓	Detail↓	Overall↑	Sharpness↓	Detail↓
HYPIR	3.00	0.92	0.75	2.79	1.07	1.14	2.70	0.30	0.70
SUPIR	2.58	0.67	0.67	2.86	1.07	0.93	3.10	0.50	0.10
PISA-SR	2.58	1.00	1.08	2.57	1.00	1.07	2.80	0.60	1.10
SeeSR	2.25	1.17	1.25	2.43	1.57	1.43	2.80	0.90	0.70
OSDiff	2.67	1.08	1.17	2.36	1.21	1.14	2.60	0.60	0.60
CCSR	2.25	1.33	1.33	2.36	1.43	1.14	2.40	0.90	1.40
DiffBIR	2.75	0.67	0.92	2.50	1.43	1.21	2.60	0.80	0.80
StablesR	2.17	1.58	1.33	1.86	2.07	1.86	2.00	1.80	1.10
PASD	2.33	0.58	0.58	2.57	1.29	1.07	2.70	1.00	0.80
Invsr	2.00	0.75	1.17	2.64	0.93	1.07	2.10	0.50	1.30
S3Diff	2.83	0.83	0.83	3.00	0.86	1.07	2.70	0.50	1.00
TSD-SR	2.58	0.67	0.75	2.71	1.07	0.93	2.50	0.70	0.70
ResShift	1.67	1.33	1.42	1.50	1.50	1.50	1.60	1.40	2.20
FLUX	1.33	1.75	1.42	0.79	2.07	2.00	0.60	2.40	1.80
Nano Banana	0.83	2.25	2.00	1.21	2.14	2.00	1.50	1.70	1.50
BSRGAN	1.92	1.58	1.33	1.36	2.14	1.86	1.70	1.50	1.80
CAL-GAN	1.58	1.42	1.17	1.14	1.71	1.79	1.60	1.30	2.07
RealESRGAN	1.92	1.08	1.33	1.79	1.50	1.29	2.10	1.40	2.00
HAT	1.75	1.67	1.42	2.07	1.71	1.57	1.80	2.00	1.80
SwinIR	2.00	1.25	1.33	2.29	1.50	1.14	2.10	0.90	1.50

Table 12. The result of average overall, sharpness, detail, and semantics scores for all restoration models in Complex Texture, Complex Texture and Fabric Texture. Note that the Detail and Sharpness scores are calculated by taking the absolute value first, and then averaging the scores.

Model	Leather Surface			Reflective Glass			Water Flow		
	Overall↑	Sharpness↓	Detail↓	Overall↑	Sharpness↓	Detail↓	Overall↑	Sharpness↓	Detail↓
HYPIR	3.50	0.33	0.17	3.21	0.64	0.64	2.40	1.30	1.30
SUPIR	3.00	0.92	0.83	2.50	0.93	0.86	2.30	1.30	1.00
PISA-SR	3.25	0.50	0.58	2.43	1.14	1.07	2.50	1.20	1.30
SeeSR	2.42	0.92	1.25	2.43	1.14	1.21	2.40	1.30	1.30
OSDiff	3.42	0.50	0.58	2.50	1.14	1.14	2.40	1.50	1.50
CCSR	2.75	0.42	0.75	1.93	1.43	1.50	2.00	1.40	1.60
DiffBIR	3.33	0.25	0.42	2.57	0.79	0.86	2.60	1.10	1.20
StablesR	2.25	1.67	1.33	1.86	1.64	1.57	1.80	2.00	1.60
PASD	3.42	0.33	0.42	3.07	0.50	0.36	3.00	0.90	0.80
Invsr	2.92	0.75	0.58	2.57	0.93	1.07	2.50	1.00	1.20
S3Diff	3.00	0.42	0.50	2.64	0.79	0.79	2.50	1.00	1.00
TSD-SR	3.08	0.58	0.42	2.64	0.71	0.86	2.40	0.90	1.10
ResShift	2.25	1.50	1.42	1.79	1.57	1.50	2.00	1.50	1.10
FLUX	1.75	1.75	1.33	1.86	1.79	1.43	0.90	1.90	1.90
Nano Banana	1.75	1.08	0.58	1.21	2.43	1.93	1.80	1.80	1.60
BSRGAN	2.00	1.58	1.50	2.29	1.21	1.36	1.30	1.90	2.00
CAL-GAN	2.25	1.67	1.42	1.64	1.50	1.64	1.20	1.90	1.70
RealESRGAN	2.33	1.33	1.25	2.36	1.36	1.29	1.40	1.80	1.60
HAT	2.25	1.33	1.58	1.93	1.71	1.71	1.60	2.00	1.80
SwinIR	2.33	1.42	1.25	2.14	1.36	1.21	1.80	1.90	2.00

Table 13. The result of average overall, sharpness, detail, and semantics scores for all restoration models in Leather Surface, Leather Surface and Water Flow. Note that the Detail and Sharpness scores are calculated by taking the absolute value first, and then averaging the scores.

Model	Vehicles			Street View			Aerial View					
	Overall↑	Sharpness↓	Detail↓	Semantics↓	Overall↑	Sharpness↓	Detail↓	Semantics↓	Overall↑	Sharpness↓	Detail↓	Semantics↓
HYPIR	2.80	1.00	1.00	2.80	2.64	1.07	1.36	2.93	2.50	1.30	1.40	2.80
SUPIR	2.70	1.00	1.00	2.60	2.43	1.07	1.07	2.43	2.40	1.60	1.00	2.40
PISA-SR	2.70	1.00	1.60	3.00	2.36	1.36	1.29	2.43	1.40	1.60	1.70	2.10
SeeSR	2.20	1.00	1.40	2.70	1.93	1.64	1.71	2.07	1.70	1.70	1.40	2.40
OSDiff	2.50	1.50	1.60	2.90	1.79	1.64	1.71	2.00	1.80	1.90	1.70	2.20
CCSR	2.50	1.30	1.20	2.60	2.21	1.43	1.36	2.71	1.70	2.20	1.80	1.90
DiffBIR	2.40	1.40	1.40	2.60	2.14	1.36	1.36	2.43	2.10	1.10	1.60	2.20
StablesR	2.00	1.70	1.60	2.50	1.64	2.00	1.71	2.14	1.80	1.90	1.50	2.50
PASD	3.10	0.60	0.70	2.90	2.21	1.00	0.93	2.29	2.90	0.70	0.60	3.00
Invsr	2.70	1.20	1.30	2.80	2.57	1.14	1.14	2.64	2.30	1.30	1.30	2.50
S3Diff	2.60	0.70	0.70	2.50	2.21	1.07	1.36	2.57	2.30	1.20	1.20	2.50
TSD-SR	2.90	1.10	1.40	2.80	2.43	0.64	1.07	2.50	2.30	1.00	1.00	2.30
ResShift	1.00	1.90	1.90	1.60	1.29	2.14	2.00	1.93	1.10	1.80	2.00	1.60
FLUX	2.40	1.00	1.00	2.60	1.50	1.86	1.57	2.14	1.30	2.10	1.60	2.10
Nano Banana	1.50	2.10	1.90	2.20	0.79	2.50	2.36	2.50	0.70	2.70	2.20	2.20
BSRGAN	1.10	1.80	1.90	1.40	1.57	2.21	2.07	2.07	1.40	1.70	1.60	2.10
CAL-GAN	1.50	1.50	1.70	1.50	1.50	1.79	1.64	2.14	1.10	1.70	1.70	1.70
RealESRGAN	1.70	1.60	1.90	2.10	2.07	1.64	1.64	2.36	0.80	1.70	1.90	1.50
HAT	1.20	2.00	2.10	1.80	1.29	1.86	1.86	1.50	1.00	1.90	2.00	1.80
SwinIR	1.60	1.60	1.90	2.00	1.57	1.43	1.71	2.21	1.70	1.50	1.80	2.20

Table 14. The result of average overall, sharpness, detail, and semantics scores for all restoration models in Vehicles, Street View and Aerial View. Note that the Detail and Sharpness scores are calculated by taking the absolute value first, and then averaging the scores.

Model	Architecture			Food			Text					
	Overall↑	Sharpness↓	Detail↓	Semantics↓	Overall↑	Sharpness↓	Detail↓	Semantics↓	Overall↑	Sharpness↓	Detail↓	Semantics↓
HYPIR	2.88	0.75	0.88	3.06	2.93	0.57	0.57	3.00	2.56	0.78	0.94	2.56
SUPIR	2.62	0.44	0.81	2.69	3.00	0.71	0.86	3.00	2.50	0.94	0.61	2.39
PISA-SR	2.44	1.06	1.19	2.69	3.07	1.07	0.79	3.14	2.33	0.94	0.94	2.61
SeeSR	2.38	1.12	1.25	2.69	2.64	0.79	0.86	2.79	1.78	1.00	0.89	1.89
OSDiff	2.81	1.06	0.94	2.81	2.57	1.14	0.93	2.79	1.94	1.28	1.28	2.06
CCSR	2.38	0.94	1.06	2.50	2.93	0.93	0.86	3.00	2.22	0.94	1.22	2.33
DiffBIR	2.62	0.81	1.00	2.75	2.93	0.71	0.79	3.00	2.22	0.72	0.72	2.22
StablesR	1.62	1.88	1.69	2.38	2.43	1.29	1.14	2.86	1.61	1.39	1.22	2.11
PASD	2.75	0.81	0.62	3.00	3.14	0.21	0.43	2.93	2.11	0.78	0.83	2.33
Invsr	2.88	1.00	1.06	3.00	2.93	0.64	0.64	2.79	2.06	0.89	0.67	2.06
S3Diff	3.00	0.62	0.50	3.06	2.86	0.50	0.71	3.00	2.33	0.78	0.67	2.28
TSD-SR	2.88	1.06	1.06	2.94	3.07	0.36	0.43	3.07	2.33	0.94	0.83	2.33
ResShift	2.00	1.44	1.44	2.38	1.93	1.79	1.21	2.57	1.28	1.56	1.33	1.61
FLUX	1.75	1.56	1.12	2.19	2.14	1.43	1.36	2.43	1.50	1.22	1.06	1.89
Nano Banana	1.44	2.06	1.88	2.38	2.00	1.64	1.57	2.50	2.00	1.39	0.94	2.33
BSRGAN	1.62	1.75	1.56	2.12	2.07	1.71	1.43	3.07	1.33	2.00	1.39	1.83
CAL-GAN	1.69	1.25	1.62	2.12	1.36	1.86	1.86	1.86	1.22	1.78	1.33	1.50
RealESRGAN	2.12	1.25	1.50	2.44	1.79	1.64	1.43	2.36	1.72	1.61	1.28	1.83
HAT	1.75	1.62	1.56	2.12	1.64	1.93	1.79	2.36	1.61	1.44	1.44	1.83
SwinIR	1.81	1.44	1.56	2.25	2.21	1.36	1.21	2.50	1.56	1.61	1.28	1.89

Table 15. The result of average overall, sharpness, detail, and semantics scores for all restoration models in Architecture, Food and Text. Note that the Detail and Sharpness scores are calculated by taking the absolute value first, and then averaging the scores.

Model	Hand-drawn			Print Media			Cartoon/Comic		
	Overall↑	Sharpness↓	Detail↓	Overall↑	Sharpness↓	Detail↓	Overall↑	Sharpness↓	Detail↓
HYPIR	3.00	0.79	0.64	2.64	0.93	0.86	2.50	0.50	0.67
SUPIR	2.00	1.57	1.14	2.29	1.21	1.21	2.07	1.08	1.00
PISA-SR	2.71	1.21	1.29	2.29	1.21	0.93	2.29	0.67	1.08
SeeSR	2.50	1.36	1.21	2.21	1.43	1.14	2.50	2.25	1.33
OSDiff	2.21	1.64	1.57	1.93	1.71	1.71	1.86	0.83	1.00
CCSR	2.07	0.93	1.21	2.07	1.00	1.07	2.29	2.83	0.92
DiffBIR	2.29	1.29	1.43	2.14	0.93	0.86	2.14	2.00	1.33
StablesR	1.71	2.14	1.43	1.71	1.79	1.36	2.00	1.67	1.17
PASD	2.50	0.86	0.86	2.86	0.79	0.86	2.71	2.75	2.83
Invsr	2.36	1.07	1.21	2.00	1.71	1.43	2.14	0.67	0.83
S3Diff	2.71	0.93	0.93	2.07	1.43	1.29	2.21	0.50	0.75
TSD-SR	2.29	1.14	1.07	2.57	0.79	0.93	2.71	2.92	2.92
ResShift	1.43	1.93	1.79	1.43	1.79	1.57	1.64	1.58	1.42
FLUX	1.79	1.29	1.29	2.43	0.93	1.14	2.50	1.08	1.08
Nano Banana	1.43	1.86	1.50	1.43	2.14	1.71	1.93	2.00	1.58
BSRGAN	1.86	1.86	1.71	1.21	2.14	2.00	1.64	1.33	1.50
CAL-GAN	1.64	1.93	1.86	1.29	1.71	1.50	1.14	1.50	1.67
RealESRGAN	1.93	1.57	1.50	1.29	1.79	1.57	1.50	1.25	1.67
HAT	1.36	1.93	2.07	1.57	1.57	1.29	1.86	1.67	1.58
SwinIR	1.93	1.43	1.43	1.43	1.79	1.50	1.64	1.08	1.42

Table 16. The result of average overall, sharpness, detail, and semantics scores for all restoration models in Hand-drawn, Hand-drawn and Cartoon/Comic. Note that the Detail and Sharpness scores are calculated by taking the absolute value first, and then averaging the scores.

Model	Compression			Defocus Blur			Digital Zoom		
	Overall↑	Sharpness↓	Detail↓	Overall↑	Sharpness↓	Detail↓	Overall↑	Sharpness↓	Detail↓
HYPIR	2.76	0.63	0.78	2.95	0.95	0.77	3.27	0.98	1.00
SUPIR	2.26	1.13	1.20	2.09	1.55	1.41	2.45	1.28	1.13
PISA-SR	2.52	1.02	1.02	2.77	0.86	0.91	3.18	1.26	1.09
SeeSR	2.17	1.28	1.43	2.18	1.23	1.27	2.55	1.57	1.65
OSDiff	2.41	1.02	1.04	2.73	0.82	0.95	3.05	2.04	2.04
CCSR	2.24	1.04	1.22	2.36	0.91	1.05	2.64	1.17	1.28
DiffBIR	2.22	1.22	1.33	2.59	0.82	1.00	2.73	1.28	1.13
StablesR	2.11	1.26	1.17	1.77	1.68	1.41	2.68	1.33	1.11
PASD	2.37	1.17	1.09	1.95	1.45	1.32	2.64	1.33	1.20
Invsr	2.30	1.04	1.09	2.32	1.09	1.05	2.73	1.41	1.33
S3Diff	1.54	1.80	1.54	2.23	1.45	1.41	2.77	2.17	2.11
TSD-SR	2.33	1.04	1.11	2.18	1.23	1.36	2.73	0.96	0.89
ResShift	1.39	1.78	1.65	1.36	2.00	1.91	2.23	1.89	1.85
FLUX	1.91	1.63	1.50	2.27	1.32	1.27	2.73	1.28	1.20
Nano Banana	2.00	1.52	1.41	1.14	2.41	2.32	1.91	1.85	1.52
BSRGAN	1.15	1.87	1.74	1.59	1.64	1.41	2.32	1.96	1.80
CAL-GAN	1.15	1.87	1.74	1.27	2.05	1.91	2.09	2.28	2.11
RealESRGAN	1.48	1.70	1.74	1.73	1.82	1.64	2.41	1.98	1.85
HAT	1.52	1.80	1.74	1.55	2.09	1.95	2.41	1.98	1.65
SwinIR	1.57	1.57	1.48	1.59	1.73	1.64	2.50	1.76	1.67

Table 17. The result of average overall, sharpness, detail, and semantics scores for all restoration models in Compression, Compression and Digital Zoom. Note that the Detail and Sharpness scores are calculated by taking the absolute value first, and then averaging the scores.

Model	ISP Noise			Low light			Motion Blur		
	Overall↑	Sharpness↓	Semantics↓	Overall↑	Sharpness↓	Semantics↓	Overall↑	Sharpness↓	Semantics↓
HYPIR	3.12	0.54	0.71	2.39	1.13	1.05	2.43	1.50	1.64
SUPIR	2.08	1.71	1.42	1.66	1.97	1.66	0.86	2.50	2.43
PISA-SR	2.75	0.96	0.88	2.45	1.21	1.08	1.43	2.14	1.57
SeeSR	1.92	1.33	1.38	1.61	1.71	1.63	1.57	2.07	2.21
OSDiff	2.67	0.71	0.92	1.97	1.34	1.21	2.00	1.86	1.64
CCSR	2.29	1.29	1.08	1.74	1.42	1.24	1.00	2.21	2.14
DiffBIR	2.67	1.00	0.92	2.05	1.42	1.37	2.14	1.57	1.50
StablesR	2.54	0.96	0.83	1.71	1.76	1.84	0.71	2.43	2.36
PASD	2.33	1.17	1.08	1.97	1.47	1.42	1.57	2.21	1.71
Invsr	2.33	1.12	1.21	1.71	1.68	1.63	1.50	2.07	2.00
S3Diff	1.46	1.79	1.50	1.24	2.16	1.76	1.14	2.29	1.86
TSD-SR	2.71	0.79	0.79	2.18	1.39	1.45	1.50	2.00	1.79
ResShift	1.46	2.00	1.88	1.13	2.03	1.92	0.64	2.64	2.50
FLUX	2.75	0.79	0.88	1.79	1.55	1.53	2.14	1.50	1.43
Nano Banana	1.62	1.50	1.38	1.66	1.84	1.55	0.57	2.64	2.29
BSRGAN	1.38	1.83	1.92	1.03	2.16	1.97	0.64	2.71	2.64
CAL-GAN	1.17	1.96	1.83	0.82	2.26	2.16	0.43	2.79	2.50
RealESRGAN	1.54	1.71	1.79	1.08	2.13	2.03	0.57	2.50	1.50
HAT	1.38	1.92	1.83	0.89	2.13	1.97	0.00	3.00	2.86
SwinIR	1.29	1.75	1.83	1.39	2.16	1.82	0.21	2.79	2.64

Table 18. The result of average overall, sharpness, detail, and semantics scores for all restoration models in ISP Noise, ISP Noise and Motion Blur. Note that the Detail and Sharpness scores are calculated by taking the absolute value first, and then averaging the scores.

Model	Old Film			Old Photo (B/W)			Old Photo (Color)		
	Overall↑	Sharpness↓	Semantics↓	Overall↑	Sharpness↓	Semantics↓	Overall↑	Sharpness↓	Semantics↓
HYPIR	2.68	0.96	0.99	2.79	0.88	0.95	2.90	0.77	0.77
SUPIR	1.69	1.90	1.65	2.12	1.38	1.19	2.16	1.47	1.37
PISA-SR	2.46	1.25	1.32	2.67	0.86	1.02	2.61	0.84	0.89
SeeSR	2.09	1.60	1.59	2.57	1.07	1.19	2.33	1.26	1.17
OSDiff	2.38	1.22	1.22	2.64	0.90	0.95	2.59	1.03	1.19
CCSR	2.07	1.38	1.46	2.41	1.07	1.10	2.33	1.14	1.21
DiffBIR	2.35	1.19	1.25	2.78	0.97	0.98	2.51	1.03	1.13
StablesR	1.63	1.90	1.74	2.50	1.22	1.21	1.89	1.53	1.50
PASD	1.81	1.59	1.47	2.64	0.98	0.93	2.49	1.03	1.01
Invsr	2.10	1.22	1.22	2.52	1.16	1.16	2.31	0.99	1.06
S3Diff	2.32	1.32	1.25	2.03	1.57	1.31	2.06	1.47	1.37
TSD-SR	2.43	1.19	1.24	2.76	0.86	0.98	2.49	1.10	1.10
ResShift	1.46	2.03	1.87	1.60	1.64	1.53	1.46	1.80	1.86
FLUX	1.97	1.54	1.41	2.21	0.81	0.78	2.19	1.23	1.13
Nano Banana	1.00	2.21	2.09	1.81	1.69	1.45	1.29	2.13	1.97
BSRGAN	1.46	2.00	1.94	1.47	1.71	1.97	1.29	1.83	1.89
CAL-GAN	1.31	2.03	1.99	1.16	1.74	1.81	1.20	2.03	1.89
RealESRGAN	1.38	2.10	1.94	1.52	1.62	1.69	1.39	1.87	1.90
HAT	1.53	2.12	1.85	1.57	1.83	1.81	1.14	1.96	1.80
SwinIR	1.38	2.01	1.93	1.88	1.55	1.55	1.51	1.80	1.83

Table 19. The result of average overall, sharpness, detail, and semantics scores for all restoration models in Old Film, Old Photo (Color). Note that the Detail and Sharpness scores are calculated by taking the absolute value first, and then averaging the scores.

Model	Surveillance			
	Overall↑	Sharpness↓	Detail↓	Semantics↑
HYPiR	2.25	1.43	1.36	2.50
SUPIR	2.00	1.57	1.39	2.29
PiSA-SR	2.00	1.64	1.54	2.46
SeeSR	2.04	1.64	1.68	2.32
OSEDiff	2.00	1.57	1.57	2.29
CCSR	1.61	1.82	1.64	1.96
DiffBiR	1.96	1.61	1.68	2.25
StableSR	1.25	2.18	2.11	1.89
PASD	2.25	1.18	1.29	2.68
Invsr	1.57	1.64	1.64	1.79
S3Diff	2.21	1.43	1.61	2.39
TSD-SR	1.79	1.61	1.61	2.11
ResShift	1.21	2.43	2.21	1.71
FLUX	1.25	2.21	1.93	1.89
Nano Banana	0.89	2.25	2.14	1.46
BSRGAN	1.43	2.21	2.14	1.96
CAL-GAN	1.00	2.18	2.11	1.61
RealESRGAN	1.39	2.18	2.07	2.21
HAT	1.25	2.36	2.11	1.89
SwimIR	1.21	2.18	2.11	2.00

Table 20. The result of average overall, sharpness, detail, and semantics scores for all restoration models in Surveillance. Note that the Detail and Sharpness scores are calculated by taking the absolute value first, and then averaging the scores.